J. Fluid Mech. (1995), *vol.* 286, *pp.* 137–171
Copyright © 1995 Cambridge University Press

Wall pressure and coherent structures in a turbulent boundary layer on a cylinder in axial flow

By STEPHEN R. SNARSKI[1] AND RICHARD M. LUEPTOW[2]

[1] Naval Undersea Warfare Center Detachment, New London, CT 06320, USA

[2] Department of Mechanical Engineering, Northwestern University, Evanston, IL 60208, USA

(Received 18 February 1994 and in revised form 16 September 1994)

Measurements of wall pressure and streamwise velocity fluctuations in a turbulent boundary layer on a cylinder in an axial air flow ($\delta/a = 5.04$, $Re_\theta = 2870$) have been used to investigate the turbulent flow structures in the cylindrical boundary layer that contribute to the fluctuating pressure at the wall in an effort to deduce the effect of transverse curvature on the structure of boundary layer turbulence. Wall pressure was measured at a single location with a subminiature electret condenser microphone, and the velocity was measured throughout a large volume of the boundary layer with a hot-wire probe. Auto- and cross-spectral densities, cross-correlations, and conditional sampling of the pressure and streamwise velocity indicate that two primary groups of flow disturbances contribute to the fluctuating pressure at the wall: (i) low-frequency large-scale structures with dynamical significance across the entire boundary layer that are consistent with a pair of large-scale spanwise-oriented counter-rotating vortices and (ii) higher frequency small-scale disturbances concentrated close to the wall that are associated with the burst–sweep cycle and are responsible for the short-duration large-amplitude wall pressure fluctuations. A bidirectional relationship was found to exist between both positive and negative pressure peaks and the temporal derivative of u near the wall. Because the frequency of the large-scale disturbance observed across the boundary layer is consistent with the bursting frequency deduced from the average time between bursts, the burst–sweep cycle appears to be linked to the outer motion. A stretching of the large-scale structures very near the wall, as suggested by space–time correlation convection velocity results, may provide the coupling mechanism. Since the high-frequency disturbance observed near the wall is consistent with the characteristic frequency deduced from the average duration of bursting events, the bursting process provides the two characteristic time scales responsible for the bimodal distribution of energy near the wall. Because many of the observed structural features of the cylindrical boundary layer are similar to those observed in flat-plate turbulent boundary layers, transverse curvature appears to have little effect on the fundamental turbulent structure of the boundary layer for the moderate transverse curvature ratio used in this investigation. From differences that exist between the turbulence intensity, skewness, and spectra of the streamwise velocity, however, it appears that transverse curvature may enhance (i.e. energize) the large-scale motion owing to the reduced constraint imposed on the flow by the smaller cylindrical wall.

1. Introduction

The pressure fluctuations at the wall beneath a turbulent boundary layer are the result of an integral effect of fluctuations in the velocity field, as described by a Poisson equation for the pressure (Willmarth 1975*b*). The fluctuating wall pressure is of interest since it is directly responsible for excitation of structural modes of vibration of bounding surfaces as well as for the direct flow noise of sonar systems. Because the wall pressure is created by the velocity fluctuations throughout the boundary layer, it is necessary to understand the structure of the turbulent boundary layer if the flow noise and vibration are to be reduced or controlled.

Historically, the turbulent boundary layer has been viewed as a spatially and temporally random fluid motion resulting from the highly agitated and apparently unpredictable motion of eddies (Hinze 1975). Over the last 25 years, however, this perspective has changed as a result of the realization that the turbulent boundary layer contains organized coherent fluid motions that are random in occurrence in space and time but similar in character, with dynamics that strongly influence the evolution of the flow. In general terms, two types of coherent structures or organized motions can be defined in the turbulent boundary layer. The first is a quasi-cyclical ordered sequence of events in the near-wall region that is responsible for the majority of turbulence production in the boundary layer (i.e. the burst–sweep cycle). The second is a large-scale motion in the outer portions of the boundary layer that scales with the boundary layer thickness, δ. Although this overall classification is straightforward, neither the exact character of the large- and small-scale motions nor the role of each in the dynamics of the turbulent boundary layer is fully understood since coherent structures of many variations have been observed in turbulent boundary layers over the last 30 years of research. Recently, Kline & Robinson (1990) and Robinson, Kline & Spalart (1990) have provided some order to this confusion by surveying the literature and classifying all the turbulent structures, events, and motions observed in flat-plate boundary layers (and turbulent channel flows) into eight categories: (i) low-speed streaks, (ii) ejections, (iii) sweeps, (iv) vortical structures (connected vortices with more than one spatial orientation, such as hairpin vortices), (v) near-wall shear layers, (vi) near-wall pressure pockets, (vii) δ-scale shear layers or 'backs', and (viii) large-scale motions (e.g. δ-scale spanwise-oriented horseshoe-shaped or mushroom-shaped vortices; bulges and deep crevices in the turbulent/non-turbulent interface). This taxonomy, although not all inclusive, is believed to contain all the significant features of the turbulent boundary layer. Although it is fairly widely accepted that these various flow structures are not independent entities but part of a larger process, the phase relation and causality of the large-scale structures (categories vi–viii) and the turbulence-generating events near the wall (i.e. the burst–sweep cycle or categories i–v) remain a subject of much controversy (Kline & Robinson 1990).

Because the fluctuating wall pressure is a volume integral of the velocity fluctuations throughout the turbulent flow, the character of the wall pressure field is a direct reflection of these organized coherent motions in the boundary layer. Accounts of the extensive research aimed at understanding the source of wall pressure fluctuations beneath turbulent boundary layers are provided in the comprehensive reviews of Willmarth (1975*a*, *b*) and the more recent review of Eckelmann (1990). The collective body of results suggests that the wall pressure is composed of at least two groups of fluctuations. The first group consists of large-scale (low-frequency) disturbances that originate from the outer portions of the boundary layer to within the unsteady potential flow. From the relative phasing of the space–time correlations of the wall

pressure and turbulent velocities, studies have indicated that these large-scale disturbances are consistent with the character of the 'wavy' turbulent/potential flow interface outside the boundary layer (Bradshaw 1967; Panton *et al.* 1980; Kobashi, Komoda & Ichijo 1984; Kobashi & Ichijo 1986) but take the form of a large rotating vortex within the boundary layer (Willmarth & Wooldridge 1963; Willmarth 1975*a*; Kobashi *et al.* 1984; Kobashi & Ichijo 1986).

The second group of pressure fluctuations consists of small-scale (high-frequency) disturbances presumably related to the burst–sweep cycle of events. These disturbances take the form of large-amplitude wall pressure fluctuations with magnitudes as large as $9p_{rms}$, which occur only a small percentage of the time but contribute significantly to the total r.m.s. wall pressure level (Emmerling 1973; Schewe 1983; Karangelen, Wilczynski & Casarella 1991). Through the use of conditional sampling techniques on simultaneously acquired pressure and velocity signals, these large-amplitude wall pressure peaks have been found to be related to shear layer structures in the buffer region that are associated with the bursting process in flat-plate turbulent boundary layers (Thomas & Bull 1983; Kobashi & Ichijo 1986; Johansson, Her & Haritonidis 1987; Haritonidis, Gresko & Breuer 1990), direct numerical simulation turbulent channel flows (Kim 1983, 1989), and turbulent pipe flows (Dinkelacker & Langeheineken 1983; Dinkelacker 1990). Karangelen *et al.* (1991) have also shown that the frequency of occurrence of large-amplitude wall pressure events in a flat-plate boundary layer is consistent with that measured for bursting events in the buffer region (Blackwelder & Haritonidis 1983). In fact, Kim (1989) has concluded that the large-amplitude wall pressure fluctuations are a 'footprint' of the bursting phenomenon.

A possible relationship between these near-wall high-amplitude pressure peaks and the large-scale structures in the outer portions of the flow was investigated by Thomas & Bull (1983). After separating their pressure signal into low-frequency and high-frequency portions, they correlated these portions of the signal and conditionally sampled the low-frequency portion on the high-amplitude (high-frequency) pressure peaks. They concluded that the low- and high-frequency disturbances were interdependent and that the large-scale structures, although phase linked to the bursting process, were not the direct cause of it. Kobashi & Ichijo (1990) also investigated the relationship between bursts and the large-scale motion by conditional sampling the velocity at $y/\delta = 1.7$ on the large-amplitude pressure fluctuations at the wall. Unlike Thomas & Bull (1983), however, they concluded that the bursts result from the interaction of the large-scale motion with the wall. The conclusion of the community-wide survey by Kline & Robinson (1990) was that although the inner and outer layers interact, they do so weakly, such that only some of the events in the inner layers are 'phase-locked to and triggered by outer region motions'.

Although, a greater understanding of the structure of the turbulent boundary layer and, hence, the character of the fluctuating wall pressure has emerged, nearly all the research has concentrated on the canonical flat-plate boundary layer. Because the bounding surface in many practical applications has transverse curvature (e.g. aircraft fuselages, ship and submarine hulls, torpedoes, missiles, and towed sonar arrays), a need exists to understand how this modified boundary condition alters the turbulence structure and, hence, the fluctuating pressure at the wall. As stated by Kline & Robinson (1990), such complex flow conditions 'act, at a minimum, as constraints on what we must be able to explain and predict in any complete view or model of turbulent boundary layers'. In this light, the present study examines the relationship between the fluctuating wall pressure and turbulent structure of a boundary layer on a cylinder in axial flow.

A comprehensive account of the research performed over the last 35 years concerning the turbulent boundary layer on a cylinder in axial flow is provided by Lueptow (1988, 1990). The character of the boundary layer depends upon the parameter δ/a, which is the ratio of the boundary layer thickness, δ, to the radius of the cylinder, a. For $\delta/a < O(1)$, transverse curvature has little effect on the character of the boundary layer compared with the flat-plate case (Willmarth *et al.* 1976; Luxton, Bull & Rajagopalan 1984; Lueptow, Leehey & Stellinger 1985). For $\delta/a > O(1)$, the effect of transverse curvature is apparent in a fuller mean velocity profile, higher coefficient of friction, and Reynolds stress that drops off more quickly with distance from the wall than in a flat-plate boundary layer (Richmond 1957: Willmarth *et al.* 1976; Lueptow *et al.* 1985). From measurements of the convection velocity, spectral density, and space–time correlation of the wall pressure, Willmarth & Yang (1970) and Willmarth *et al.* (1976) concluded that the pressure-producing eddies in the cylindrical boundary layer ($\delta/a \approx 2$ and 4) are smaller due to the transverse shearing action that results from the limited lateral extent of the cylindrical boundary layer. For large ratios of δ/a, the boundary layer thickness can be much greater than the cylinder itself, such that the outer flow becomes increasingly independent of the wall. Measurements in cylindrical boundary layers with $\delta/a > 20$ (Luxton *et al.* 1984; Lueptow & Haritonidis 1987; Bull & Dekkers 1993) have revealed that large-scale structures can move relatively freely with little influence of the wall. However, because (i) the distance from the wall for the maximum turbulence intensity (Lueptow *et al.* 1985), (ii) the character of the ensemble-averaged events detected using variable interval time averaging (VITA) (Lueptow & Haritonidis 1987), and (iii) the near-wall streaky structure (Lueptow & Jackson 1991) are similar to those found in flat-plate boundary layers, transverse curvature apparently does not affect the turbulence-generating events near the wall.

Although previous research has been performed to study the fluctuating wall pressure and the turbulent structure of a boundary layer on a cylinder in axial flow, the fluctuating wall pressure and turbulent velocity field were considered separately. In this paper, therefore, results of simultaneous measurements of the fluctuating wall pressure and streamwise turbulent velocity in the boundary layer on a cylinder in axial flow are presented. The data considered here are those reported in complete detail by Snarski (1993, see also Snarski 1992). The transverse curvature ratio for the boundary layer examined is $\delta/a = 5$, which is well within the range where transverse curvature affects the character of the boundary layer. Through the use of turbulence statistics, auto- and cross-spectral densities, cross-correlations, and conditional sampling of the pressure and velocity signals, the relationships between the fluctuating wall pressure and fluctuating streamwise velocities throughout the boundary layer are established so that the turbulent flow structures in the cylindrical boundary layer that contribute to the fluctuating pressure at the wall can be determined. By comparing to results for flat-plate boundary layers, the effect of transverse curvature on the structure of the turbulent boundary layer is deduced.

2. Experiments

2.1. *Flow facility and measurement techniques*

The low-speed low-noise wind tunnel used for this investigation is shown in figure 1. The 3.05 m long test section was constructed with a vertical orientation to eliminate boundary layer symmetry problems associated with cylinder sag and a slightly divergent 0.35 m square cross-section to minimize the streamwise pressure gradient.

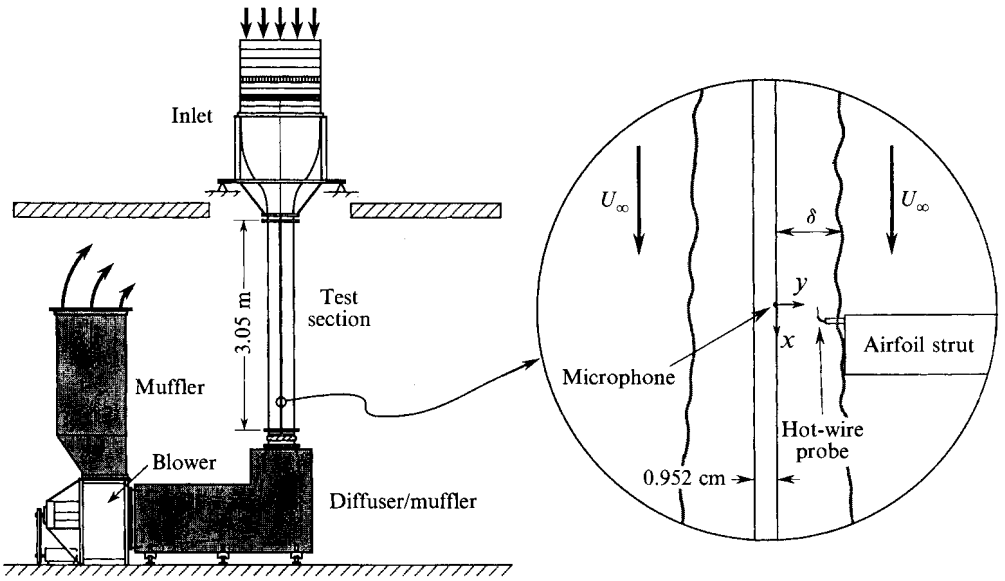

FIGURE 1. Vertical wind tunnel facility and experimental apparatus.

The inlet to the test section consists of a settling chamber with nine screens and a honeycomb for turbulence management followed by a 10.8:1 contraction section. Contamination of the wall pressure measurements by blower noise was reduced by use of a low-sound-power airfoil-vane centrifugal blower located downstream of the test section, an acoustic-muffler diffuser with a 90° elbow, and an acoustic muffler at the outlet of the blower.

The test cylinder was made from a 3 m long, 0.952 cm OD ($\frac{3}{8}$ in.) brass tube fitted with 4 cm long brass ellipsoidal cones on the nose and tail. The cylinder was suspended along the centreline of the test section by means of a 0.1 cm diameter steel cable that ran to a structural airfoil located within the inlet section. The cylinder was placed under tension and accurately positioned to ensure that the axis of the cylinder was straight and aligned with the mean flow.

The fluctuating wall pressure was measured at a distance of $X_p = 2.48$ m downstream of the boundary layer trip with a Knowles EM-3068 subminiature hearing-aid microphone. This streamwise distance corresponds to approximately 1950 trip heights. The microphone was an electret condenser type with a pinhole diameter of $d =$ 0.07 cm, corresponding to $d^+ = du_\tau/\nu = 25.9$. This is small enough to provide sufficient spatial resolution over the frequency range considered (Schewe 1983; Lueptow 1993). Although the use of pinhole microphones has been associated with increased high-frequency spectral levels (Bull & Thomas 1976), they are generally believed to be effective for wall pressure measurements (Farabee 1986; Gedney & Leehey 1989; Farabee & Casarella 1991), as long as the Helmholtz resonance frequency for the pinhole system is above the frequency range of interest, as was the case for this investigation. The frequency response (magnitude and phase) for the Knowles microphone was obtained by performing a comparison calibration in a diffuse sound field with a Bruel and Kjaer type 4138 $\frac{1}{8}$ in. pressure-response microphone (Snarski 1993). Electrical noise limited the useful frequency range of the microphone to 6700 Hz.

Mean and fluctuating streamwise velocities were measured using a home-built hot-wire probe mounted on the end of a streamlined strut that was attached to an external

Experimental conditions	Boundary layer parameters	Wall shear parameters
$U_\infty = 11.4$ m s^{-1}	$\delta = 0.024$ m	$\tau_w = 0.369$ Pa
$\lvert dC_p/dx\rvert < 0.013$ m^{-1}	$\delta^* = 4.26 \times 10^{-3}$ m	$u_\tau = 0.552$ m s^{-1}
$\rho = 1.21$ kg m^{-3} (18 °C)	$\theta = 3.75 \times 10^{-3}$ m	$u_\tau/U_\infty = 0.0484$
$\nu = 14.9 \times 10^{-6}$ m^2 s^{-1} (18 °C)	$\delta/\delta^* = 5.63$	$\nu/u_\tau = 26.9$ μm
$X_p = 2.48$ m (tripped)	$H = \delta^*/\theta = 1.14$	$\nu/u_\tau^2 = 48.9$ μs
$a = 4.76 \times 10^{-3}$ m ($a^+ = 177$)	$\delta/a = 5.04$	$Re_\tau = \delta u_\tau/\nu = 892$
$Re_x = U_\infty X_p/\nu = 1.90 \times 10^6$	$\delta^*/a = 0.895$	
$Re_a = U_\infty a/\nu = 3644$	$Re_\theta = U_\infty \theta/\nu = 2870$	

Resolution parameters		
digital	microphone	hot wire
$f_s = 20000$ Hz ($\Delta t = 50$ μs)	$d^+ = du_\tau/\nu = 25.9$	$l^+ = lu_\tau/\nu = 18.5$
$\Delta f = 19.53$ Hz	$d/\delta^* = 0.164$	
$\Delta t^+ = (\Delta t)\, u_\tau^2/\nu = 1.02$	$d^* = d^+(u_\tau/U_\infty) = 1.25$	

TABLE 1. Experimental conditions and flow parameters

computer-controlled traversing mechanism. The hot-wire probe consisted of a 2.5 μm diameter, 0.51 mm long, Pt–Rh (90/10) alloy sensing wire soldered to the tips of two jeweller's broaches. The hot-wire length of $l^+ = 18.5$ and length-to-diameter ratio of 204 provided sufficient spatial resolution and accuracy (Johansson & Alfredsson 1983).

For this investigation, the wall pressure was measured at a single fixed location on the surface of the cylinder wall, while the turbulent streamwise velocity was measured at 72 separate positions in the radial–streamwise plane containing the microphone. The measurements spanned a distance of $0 \leqslant x/\delta \leqslant 1.52$ in the streamwise (axial) direction and $0.016 \leqslant y/\delta \leqslant 1.91$ ($14 \leqslant y^+ \leqslant 1693$) in the wall-normal (radial) direction.

The data were acquired using a Macintosh IIcx computer equipped with a MacADIOS II 12-bit data-acquisition board manufactured by GW Instruments, Inc. The microphone and hot-wire signals were sampled simultaneously for 4.1 s at a sampling frequency of $f_s = 20$ kHz (81920 samples) after passing through an antialiasing filter with a cutoff frequency of 10 kHz. Longer wall pressure signals sampled for 26.2 s at 20 kHz (524288 samples) were used for the statistical and autospectral results in §§3.1 and 3.3. The time-series data were digitally filtered by applying a rectangular bandpass filter in the frequency domain ($58.59 < f < 5332$ Hz) to remove the influence of acoustic and electrical noise (see §2.3). Fast Fourier transforms were computed by applying a Hanning window to 80 subrecords (512 for the longer pressure signals) of 1024 points each, with a resulting frequency resolution of $\Delta f = 19.53$ Hz. All spectra shown are single sided.

2.2. *The turbulent boundary layer*

All measurements were carried out at a free-stream velocity of $U_\infty = 11.4$ m s^{-1}. To ensure a fully developed turbulent boundary layer at the measurement location, the boundary layer was tripped by placing a 0.13 cm thick rubber O-ring around the cylinder at the trailing edge of the brass ellipsoidal nose cone. Details of the flow conditions at the axial location of the wall pressure transducer are shown in table 1. The mean wall shear stress was determined from a Preston tube measurement of the dynamic pressure within the wall region (Preston 1954) and from Head & Ram's (1971) tabulated version of the flat-plate calibration data of Patel (1965). The flat-plate calibration data could be used for the cylindrical boundary layer since the Preston tube

was contained within a region near the wall where the cylindrical boundary layer velocity profile is adequately approximated by the flat-plate law of the wall (Willmarth *et al.* 1976; Snarski 1993; Wietrzak & Lueptow 1994). Extreme care was taken to accurately centre and align the cylinder to within 0.5 mm over the 3 m length of the cylinder (or to within 0.01° of the mean flow direction) to ensure that the boundary layer was axisymmetric. Wall pressure and wall shear stress measurements around the cylinder circumference revealed a maximum variation of 3.7% in the r.m.s. wall pressure and 2.5% in the mean wall shear stress.

2.3. *Extraneous disturbances*

Extraneous factors unrelated to the physics of the turbulent boundary layer flow can influence the measured wall pressure and streamwise velocity fluctuations as well as the relationships between them. Those of greatest significance to the present investigation are free-stream turbulence, ambient sound, cylinder vibration, and hot-wire/microphone interference. Although extreme care was taken to design a low-turbulence settling chamber and contraction section, the structural airfoil required to support the cylinder under tension introduced some vorticity into the flow. The resulting turbulence intensity at the axial position of the pressure measurements was 0.15%. The ambient sound field in the test section, measured with a Bruel and Kjaer UA 0436 Turbulence Screen at a free-stream velocity of 11.4 m s^{-1}, indicated that nearly all the ambient sound energy was below 60 Hz. As a result, pressure and velocity data below 58.59 Hz ($3\Delta f$) were not used in the analysis.

Vibration of the cylinder during the pressure–velocity measurements could affect the measured correlation through the introduction of spurious pressure signals (either by inertial effects on the microphone diaphragm or by pressures induced at the surface of the cylinder) or velocity fluctuations in the adjacent fluid. Measurements with a Knowles BU-1771 ceramic vibration transducer mounted inside the cylinder adjacent to the microphone indicated that the wall pressure and the streamwise velocity were unaffected by cylinder vibration.

Finally, close proximity of the hot-wire prove and the pinhole microphone could affect the correlation measurements by disturbances introduced into the flow from either device. When the hot wire was located immediately above the microphone ($x = 0$) and at the two closest measurement positions from the wall ($y^+ = 14, 28$), the presence of the hot wire slightly increased the wall pressure spectral levels below 800 Hz. This greater spectral energy was probably a result of the adjusted flow around the hot wire impinging on the wall and introducing more positive pressure fluctuations, as evidenced by a positive skewness in contrast to the negative skewness that occurred without the hot wire. However, because the increase in the r.m.s. wall pressure level was small, the impact of the hot wire on the interpretation of the near-wall results was not considered significant. Velocity spectra measured with the hot wire immediately above the pinhole microphone ($x = 0$) and with a spanwise displacement of the hot wire were identical within experimental uncertainty, indicating that the pinhole had no significant effect on the velocity field.

Correlated electrical noise was also present in the pressure and velocity measurements above 5350 Hz; hence, all pressure and velocity data above 5332.0 Hz ($273\Delta f$) were discarded.

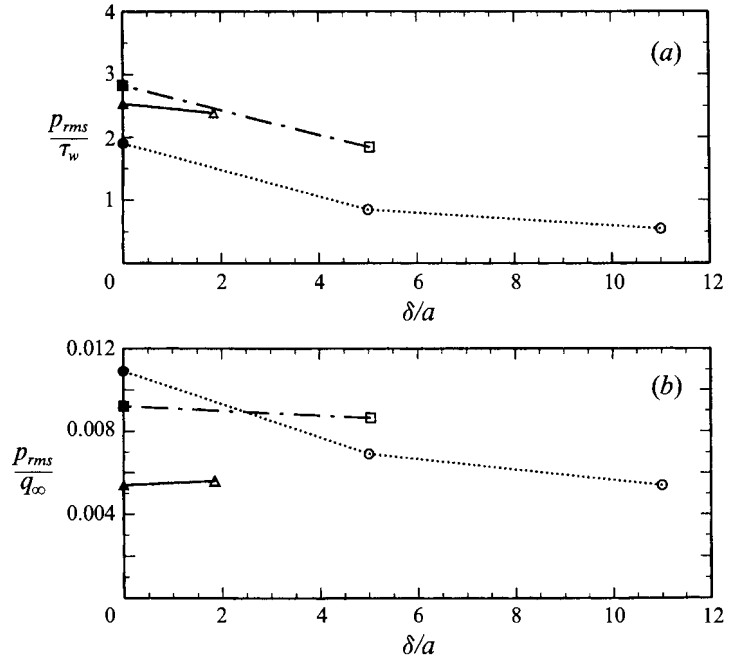

FIGURE 2. Root-mean square wall pressure (p_{rms}) as a function of transverse curvature (δ/a) non-dimensionalized on (*a*) mean wall shear stress (τ_w) and (*b*) free-stream dynamic pressure (q_∞), —·—·—; medium Re_θ, medium d^+, pinhole: □, present, $Re_\theta = 2870$, $d^+ = 25.9$ ($0.14 < \omega\delta^*/U_\infty < 12.5$); ■, Farabee (1986), $Re_\theta = 3400$, $d^+ = 33.3$ ($0.09 < \omega\delta^*/U_\infty < 36.4$). ——, large Re_θ, large d^+, flush: △, Willmarth & Yang (1970), $Re_\theta = 26200$, $d^+ = 158$ ($0.063 < \omega\delta^*/U_\infty < 57.6$); ▲, Willmarth & Roos (1965), $Re_\theta = 38000$, $d^+ = 203$ ($0.14 < \omega\delta^*/U_\infty < 28.8$). ·····, small Re_θ, small d^+, direct numerical simulation: ○, Neves *et al.* (1991), $Re_\theta = 400$, $d^+ \approx 6$; ●, Spalart (1988), $Re_\theta = 300$, $d^+ \approx 13$.

3. Results and discussion

3.1. *Wall pressure statistics*

The r.m.s. wall pressure for the present investigation measured in the frequency band $0.13 \leqslant \omega\delta^*/U_\infty \leqslant 12.5$ was 0.679 Pa. This frequency range is comparable to that used in other wall pressure investigations (Willmarth & Wooldridge 1963; Bull 1967; Willmarth & Yang 1970; Farabee 1986; Karangelen *et al.* 1991). Non-dimensionalized by the free-stream dynamic pressure and the mean wall shear stress, the r.m.s. levels are $p_{rms}/q_\infty = 8.64 \times 10^{-3}$ and $p_{rms}/\tau_w = 1.84$, respectively. These r.m.s. wall pressure levels are compared to experimental and direct numerical simulation results in figure 2 as a function of the transverse curvature δ/a. Lines connect data obtained under similar conditions (Reynolds number, transducer resolution, and transducer type). In figure 2(*a*), all three curves show a decrease in p_{rms}/τ_w with increased transverse curvature. However, because the coefficient of friction $C_f = \tau_w/q_\infty$ increases with transverse curvature (Lueptow 1990), the r.m.s. wall pressure levels are more effectively compared by non-dimensionalizing with q_∞, as shown in figure 2(*b*). Here, the effect of transverse curvature is less clear. Although the present measurements and the numerical results of Neves, Moin & Moser (1992, see also Neves, Moin & Moser 1991) still reveal a decrease in r.m.s. pressure with transverse curvature, the decrease for the present results is only 6%, while the Willmarth data actually show an increase. Although the Willmarth result may be related to the larger transducer size for the flat-plate measurements of Willmarth & Roos (1965) and the relatively small transverse

Investigation	d^+	Microphone type	Re_θ	δ/a	a^+	Skewness	Flatness	p_{rms}/q_∞ (uncorrected)
Present investigation	26	pinhole	2870	5	177	−0.08	5.05	8.64×10^{-3}
Neves *et al.* (1992)	8[a]	DNS[b]	414	5	43	−0.70	7.16	6.78×10^{-3}
Neves *et al.* (1992)	4[a]	DNS[b]	448	11	21	−0.78	6.18	5.67×10^{-3}
Schewe (1983)	19	flush	1400	flat plate		−0.18	4.90	9.8×10^{-3}
Johansson *et al.* (1987)	65	flush	4940	flat plate		0.05	3.80	7.8×10^{-3}
Haritonidis *et al.* (1990)	56	flush	4340	flat plate		0.20	3.91	NA
Wilczynski & Casarella (1992)	34	pinhole	2945	flat plate		−0.15	4.90	11.4×10^{-3}
Kim (1989)	11[a]	DNS[b]	283	channel		−0.10	5.00	8.45×10^{-3}
Neves *et al.* (1992)	12[a]	DNS[b]	287	channel		−0.03	5.16	9.16×10^{-3}

[a] Based on equivalent diameter.
[b] Direct Numerical Simulation.
NA: not available.

TABLE 2. Comparison of wall pressure statistics in cylindrical and flat plate turbulent boundary layers and turbulent channel flows

curvature for the measurements of Willmarth & Yang (1970), the collective body of data does not sufficiently illustrate the effect of transverse curvature on the r.m.s. wall pressure level.

The skewness and flatness of the wall pressure for the present investigation are compared to other available experimental and direct numerical simulation (DNS) results for cylindrical and flat-plate turbulent boundary layers as well as for turbulent channel flows in table 2. Consistent with most of the other reported wall pressure statistics, the present measurements have negative skewness (indicating that negative excursions from the mean are more likely than positive excursions) and a flatness greater than 3 (indicating that large-amplitude fluctuations from the mean occur more frequently than for a Gaussian signal). Although accounting for transducer spatial resolution reduces some of the scatter in these higher-order statistics (Schewe 1983), the data are too sparse to separate effects due to transverse curvature from those due to external disturbances (acoustic contamination, surface discontinuities, probe interference, etc.), frequency filtering, or Reynolds number.

3.2. *Streamwise velocity statistics*

The streamwise velocity statistics reported in this section were computed without any digital filtering to facilitate comparison to other measurements. Although the measurements made outside of the boundary layer ($y/\delta > 1$) were contaminated below 40 Hz ($\omega\delta^*/U_\infty = 0.094$), filtering of the extraneous energy had a negligible effect on the velocity statistics other than to decrease the r.m.s. energy level.

Distributions of the first four moments of the streamwise velocity are presented in figure 3. In figure 3(*a*), the mean velocity profile is compared to the flat-plate law of the wall as tabulated by Coles (1955). The cylindrical boundary layer profile is fuller than the flat-plate profile with a logarithmic region slope that decreases with δ/a – a consequence of the increased coefficient of friction and in agreement with previous measurements (Willmarth *et al.* 1976; Lueptow *et al.* 1985). Distributions for the next three moments are compared to measurements in a flat-plate boundary layer at $Re_\theta = 4940$ (Haritonidis *et al.* 1990) and a cylindrical boundary layer ($\delta/a = 7.2$) at $Re_\theta = 3300$ (Lueptow 1986) in figures 3(*b*)–3(*d*).

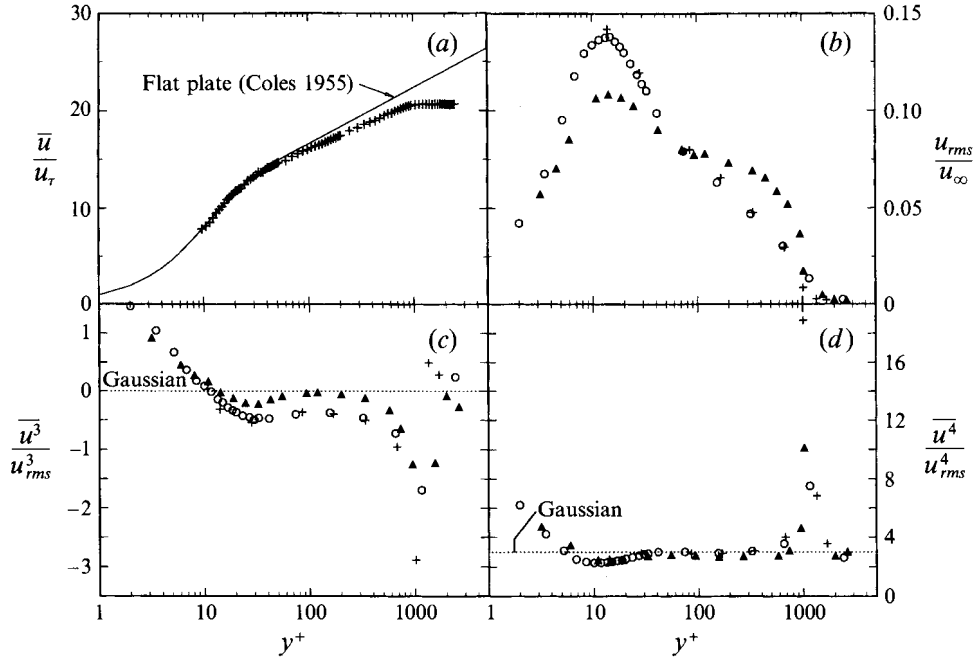

FIGURE 3. Streamwise velocity statistics: (*a*) mean velocity profile, (*b*) turbulence intensity, (*c*) skewness, and (*d*) flatness. +, Present study, $\delta/a = 5.0$, $Re_\theta = 2870$; ○, Lueptow (1986), $\delta/a = 7.2$, $Re_\theta = 3300$; ▲, Haritonidis *et al.* (1990), $\delta/a = 0$, $Re_\theta = 4300$.

The streamwise turbulence intensities non-dimensionalized by U_∞ in figure 3(*b*) for both cylindrical boundary layer measurements are lower than the flat-plate boundary layer intensities throughout most of the boundary layer ($y^+ > 85$). These reduced turbulence intensities throughout the bulk of the boundary layer are a likely result of the reduced surface area of the cylinder introducing less vorticity per unit volume into the cylindrical boundary layer compared with the flat-plate boundary layer. Near the wall ($y^+ < 85$), however, the turbulence intensities in the cylindrical boundary layer exceed the flat-plate values. Luxton *et al.* (1984) found a similar result and argued that since the wall of the cylindrical boundary layer provides less constraint on the outer flow and motion of eddies, the increased turbulence intensities near the wall can be expected due to the passage of large-scale outer structures very near the wall. Although previous investigations have compared cylindrical and flat-plate boundary layer turbulence intensity profiles in inner variables (u_{rms}/u_τ) (Afzal & Singh 1976; Lueptow & Haritonidis 1987; Neves *et al.* 1991, 1992; Luxton *et al.* 1984), the scaling does not accurately reflect the effect of transverse curvature since the inner velocity scale u_τ is itself a function of transverse curvature.

For both the cylindrical and flat-plate boundary layers, the skewness in figure 3(*c*) is negative throughout most of the boundary layer, with a sharp negative peak due to intermittency near the edge of the boundary layer. A notable difference between the cylinder and flat plate is that the cylindrical boundary layer measurements are more negatively skewed than those of the flat plate throughout the entire boundary layer. Luxton *et al.* (1984) found an even more negative skewness that tended toward -1 for $\delta/a > 20$. This indicates that negative excursions of streamwise velocity from the mean ($u < 0$), which result predominantly from ejections ($v > 0$) for $y^+ < 100$ and inward interactions ($v < 0$) for $y^+ > 100$ in flat-plate boundary layers (Robinson 1990), occur more frequently in the boundary layer with transverse curvature. Bull & Dekkers

(1993) have attributed the negative streamwise velocity fluctuations in the cylindrical boundary layer to spots of low-speed fluid distributed throughout the boundary layer that consist of low-speed inner fluid which has been stripped away from the cylinder surface by large-scale crossflows. The flatness distributions in figure 3(*d*) are very similar for both the cylindrical and flat-plate boundary layers, remaining very near the Gaussian value of 3 throughout most of the boundary layer, except near the edge where a peak occurs due to the large fluctuations in u that result from the intermittency. For $\delta/a > 20$, the flatness has been shown to increase to 5 or greater throughout the bulk of the layer (Luxton *et al.* 1984).

3.3. *Wall pressure spectrum*

The power spectral density of the fluctuating wall pressure is shown in figure 4. Because of practical problems, including free-stream turbulence, acoustic background noise, spatial resolution of transducers, and differences in transducer types (pinhole and flush-mounted) and Reynolds numbers, accurate measurement and comparison of wall pressure spectra are difficult (Keith, Hurdis & Abraham 1992; Farabee & Casarella 1991). To minimize these difficulties, the present measurements are compared to flat-plate boundary layer measurements (Farabee 1986) obtained with a similar transducer resolution, microphone type (pinhole), and Reynolds number ($Re_\theta = 3400$). Although $d^+ = du_\tau/\nu$ has traditionally been used as the spatial resolution parameter related to the high-frequency attenuation of the spectra, more appropriate spatial resolution parameters are d/δ^* for outer scalings and $d^* = \mathrm{d}^+(\mathrm{u}_\tau/U_\infty)$ for inner scalings (Keith *et al.* 1992). All three parameters are listed in figure 4 for both sets of measurements.

Because the fluctuating wall pressure results from an integral effect of turbulence across the entire boundary layer, spectral contributions at different frequencies can be related to different locations in the boundary layer. When scaled on outer variables, the spectra for flat-plate boundary layers obtained at widely varying flow conditions collapse at low frequencies, suggesting that low-frequency spectral energy is associated with the large-scale structures in the outer portions of the boundary layer (Farabee & Casarella 1991; Keith *et al.* 1992). When scaled on inner variables, these spectra collapse at high frequencies, after transducer resolution effects and transducer type are taken into account, suggesting that spectral energy at high frequencies is related to small-scale turbulent fluctuations in the near-wall region of the boundary layer (Farabee & Casarella 1991; Keith *et al.* 1992). Since all the experimental conditions in figure 4 are similar except for transverse curvature, the inner and outer scalings had a negligible effect on the relative spectral magnitudes between the two sets of measurements; hence, the spectra were simply normalized by p_{rms}^2 and scaled using outer velocity and length scales. Because δ^* as well as δ and the other integral length scales for the boundary layer decrease with transverse curvature due to the larger skin friction and, hence, fuller mean velocity profile (White 1972), the appropriate length scale to use for comparison is unclear. Results using both δ^* and δ are shown in figure 4.

In the scaling based on δ^*, the present measurements have a smaller energy content than the flat-plate boundary layer spectrum at low frequencies ($\omega\delta^*/U_\infty < 1$) and a greater energy content at higher frequencies ($\omega\delta^*/U_\infty > 5$). This result is consistent with the findings of Willmarth & Yang (1970) and Willmarth *et al.* (1976) for cylindrical boundary layer wall pressure spectra with $\delta/a \approx 2$ and 4. Willmarth & Yang (1970) used this 'shifting of energy to higher frequencies' to support their assertion that the pressure-producing eddies in the cylindrical boundary layer are smaller than those in a flat-plate boundary layer. However, if the cylindrical and flat plate results in figure

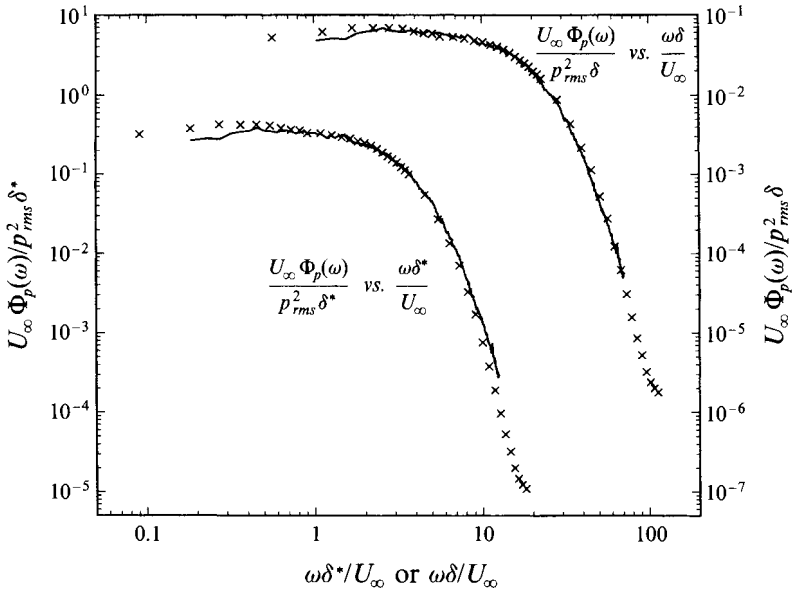

FIGURE 4. Comparison of fluctuating wall pressure spectra in outer scalings for cylindrical and flat plate boundary layers. ——, Present, $\delta/a = 5.0$, $Re_\theta = 2870$, $d/\delta^* = 0.164$, $d^+ = 25.9$, $d^* = 1.25$; ×, Farabee (1986), $\delta/a = 0$, $Re_\theta = 3400$, $d/\delta^* = 0.177$, $d^+ = 33.3$, $d^* = 1.32$.

4 are instead compared in the scaling based on δ, the spectral densities for the present measurements collapse at nearly all frequencies. This suggests that the distribution of wall pressure energy with frequency is not significantly affected by transverse curvature. However, whether this collapse or the shift of energy to higher frequencies is the correct interpretation cannot be determined since both δ and δ^* are functions of transverse curvature. Because the ratio δ/δ^* is smaller in a cylindrical boundary layer than a flat-plate boundary layer – an effect that can be explained by the larger coefficient of friction C_f in the cylindrical boundary layer and the equilibrium boundary layer relation $\delta/\delta^* \approx 0.26(C_f/2)^{-1/2}$ of Coles (1956) – non-dimensionalizing the spectra via δ rather than δ^* causes a clockwise rotation of the cylindrical spectrum relative to the flat-plate spectrum since the abscissa is multiplied by the length scale and the ordinate is divided by it.

3.4. *Streamwise velocity spectra*

The power spectral density of the streamwise velocity at nine wall-normal locations in the cylindrical boundary layer are shown in figure 5. Because the data set size was smaller than for the wall pressure spectrum, frequency smoothing was used to minimize the random error in the spectral estimate (Bendat & Piersol 1986). The spectra are plotted in the form of dimensional first-moment spectral densities $\omega\Phi_u(\omega)$ versus $\log\omega$ to emphasize the differences between velocity measurements at different locations in the boundary layer (Samuel & Joubert 1974; Bullock, Cooper & Abernathy 1978; Farabee 1986). Because traditional log–log $\Phi_u(\omega)$ spectral density plots do not provide a good visual indication of the relative contribution of each frequency range to the total mean square energy level, Bradshaw (1971) suggested this plot format as an alternative, since $u_{rms}^2 = \int \omega\Phi_u(\omega)\,\mathrm{d}(\ln\omega) = \int \Phi_u(\omega)\,\mathrm{d}\omega$ and equal areas under different portions of the curve contribute equally to the mean square energy.

The general character of the spectra in figure 5 is similar to what has been observed in flat-plate boundary layers (Farabee 1986; Farabee & Casarella 1991; Wilczynski &

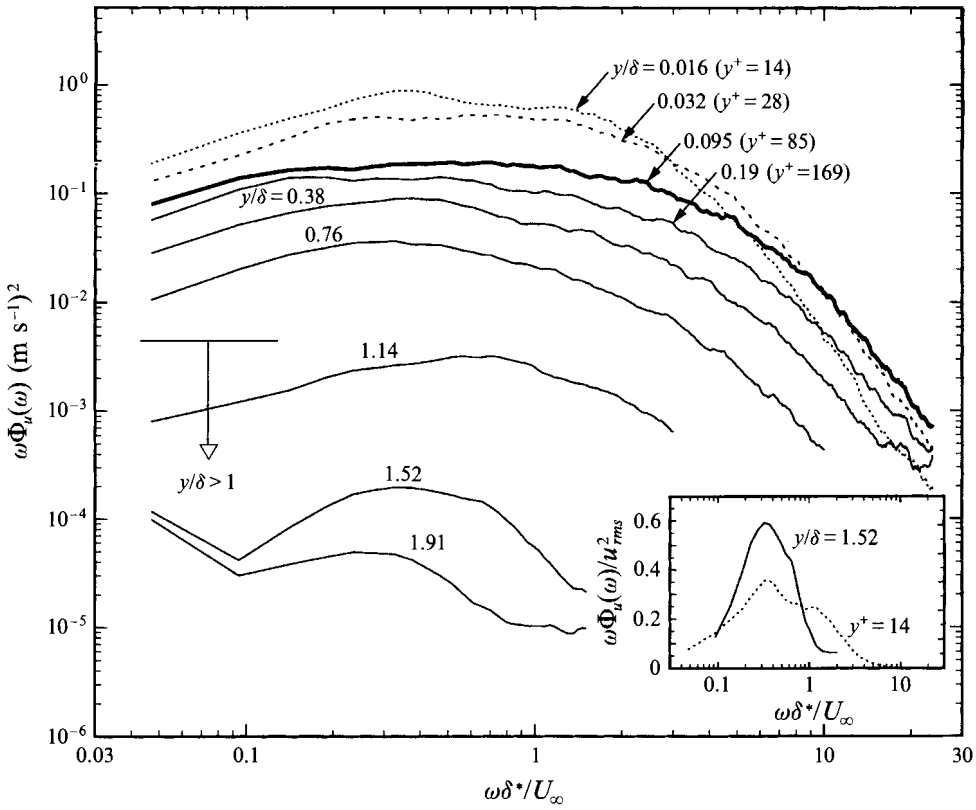

FIGURE 5. First-moment spectral density of the streamwise velocity across the boundary layer.

Casarella 1992). Within the boundary layer ($y/\delta < 1$), the spectra are broadband, typical of turbulence spectra, while those outside the boundary layer ($y/\delta > 1$) are more band-limited in character, representative of the organized irrotational motion of the turbulent/potential-flow interface (Farabee & Casarella 1991). As the wall is approached from the edge of the boundary layer, the spectral levels monotonically increase at all frequencies down to the measurement at $y/\delta = 0.095$ ($y^+ = 85$), where the spectral levels at the highest frequencies reach a maximum and then begin to decrease as the hot wire is moved closer to the wall. This indicates that all frequencies contribute to the increase in turbulence intensity in figure 3(*b*) as the wall is approached down the point $y^+ = 85$, while consistently lower and lower frequencies are responsible for the increase at positions closer to the wall. Because the turbulence intensity for the cylindrical boundary layer exceeds that for the flat-plate boundary layer below $y^+ = 85$, this result provides evidence that the large-scale motion is more energetic near the wall in the cylindrical boundary layer as suggested by Luxton *et al.* (1984). Very similar spectral variations can be seen in the cylindrical boundary layer spectra of Lueptow & Haritonidis (1987) and can be deduced from the flat-plate spectra of Klebanoff (1957) in which maximum high-frequency spectral energy levels occur for their measurements at $y^+ = 78$ and 137, respectively. This suggests that for both flat-plate and cylindrical boundary layers, the wall has a spatial-filtering effect on the near-wall flow ($y^+ < \sim 100$), attenuating longer and longer wavelengths as the wall is approached until the longest wavelengths are eliminated at the wall where the turbulence intensity goes to zero.

If the character of the velocity spectra in figure 5 is examined more closely, the velocity spectrum measured at $y/\delta = 0.016$ ($y^+ = 14$) contains two small humps at $\omega\delta^*/U_\infty \approx 0.35$ and 1.22. This is illustrated more clearly after normalization by u^2_{rms} in the inset to figure 5. A similar double-hump structure has been observed in near-wall first-moment velocity spectra in flat-plate boundary layers (Bullock *et al.* 1978; Farabee 1986) and pipe flows (Perry & Abell 1975). A double-humped structure can also be detected in the near-wall cylindrical boundary layer spectra of Luxton *et al.* (1984) ($y^+ \approx 6$, $\delta/a = 26.7$, $Re_\theta = 2990$) at frequencies similar to those found here. Because equal areas under different portions of first-moment spectral densities contribute equally to the mean square energy, spectral humps or peaks occur at frequencies where the greatest contribution to the mean square energy occurs for any constant percentage (logarithmic) bandwidth $\mathrm{d}(\log\omega)$. Assuming that such spectral humps are associated with some characteristic feature of the turbulent flow, the double-hump structure near the wall suggests that two characteristic flow scales exist in the near-wall region of all wall-bounded turbulent flows. Because the lower frequency hump at $\omega\delta^*/U_\infty \approx 0.35$ in the spectrum at $y^+ = 14$ occurs at the same frequency as the peak in the velocity spectrum at $y/\delta = 1.52$ (see inset to figure 5), the two disturbances may be related. Furthermore, since the spectral peak at $y/\delta = 1.52$ is associated with the organized irrotational motion of the turbulent/potential-flow interface, the low-frequency hump or characteristic scale near the wall may be associated with the large-scale motion. More evidence for this is provided by results and a conceptual model presented later. Strickland & Simpson (1975) observed peaks in the first-moment spectral density of the wall shear stress in a flat-plate boundary layer at low frequencies and suggested that the peak was related to the statistically periodic phenomenon of bursting. If this is true, these results may provide evidence that the burst–sweep cycle is coupled to the large-scale structure in the boundary layer. More insight into this coupling as well as the source of the high-frequency spectral peak near the wall are provided in later sections.

The first-moment velocity spectra were also compared directly to flat-plate boundary layer spectra with a similar Reynolds number, boundary layer thickness, and hot-wire resolution (Wilczynski & Casarella 1992) at four locations across the boundary layer ($y^+ \approx 90$ to $y/\delta \approx 1.1$). Although the first-moment spectral densities are similar in character for both boundary layers, the spectra for the present measurements are more peaked than those for the flat-plate measurements owing to a greater fraction of the total energy near the spectral peak and a smaller fraction at low frequencies ($\omega\delta^*/U_\infty < 0.1$) for $y/\delta \leqslant 0.7$ and at high frequencies ($\omega\delta^*/U_\infty > 2$) for $y/\delta \geqslant 0.7$. An effect similar to that found here for $y/\delta \leqslant 0.7$ can be deduced from the measurements of Afzal & Singh (1976) in which they compared their cylindrical boundary layer velocity spectra to the flat-plate spectra of Klebanoff (1957). Such a focusing of energy to the first-moment spectral peak could be a result of the less constrained and, therefore, more energetic motion of the large-scale structures in the cylindrical boundary layer.

3.5. *Pressure–velocity cross-spectra*

The cross-spectrum, $\Phi_{pu}(\omega)$, provides the relationship between the pressure and the streamwise velocity as a function of frequency. Because the cross-spectrum is a complex function, the results in this section are presented in terms of the coherence, or normalized cross-spectral magnitude, defined by

$$\Gamma_{pu}(\omega) = \frac{|\Phi_{pu}(\omega)|}{[\Phi_p(\omega)\,\Phi_u(\omega)]^{1/2}}, \tag{1}$$

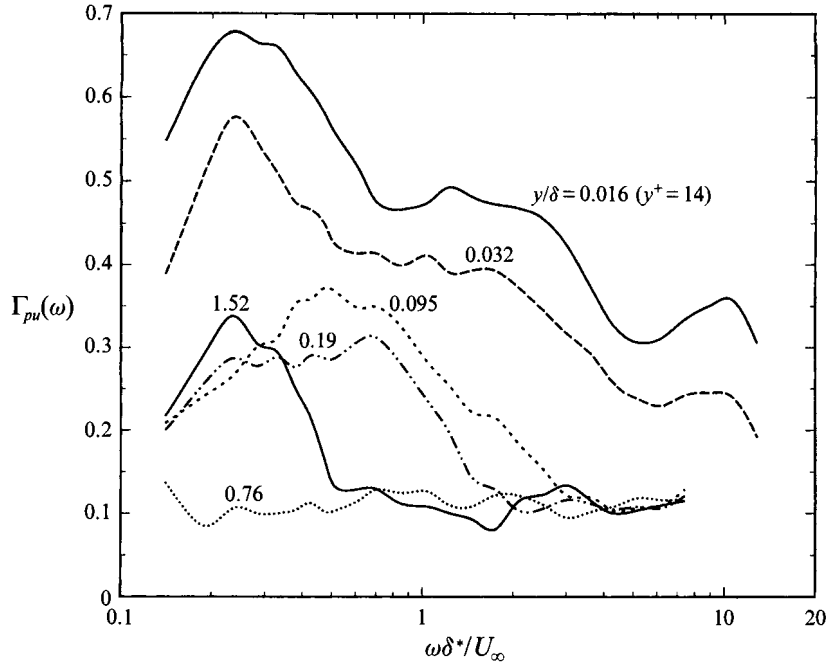

FIGURE 6. Coherence between the wall pressure and streamwise velocity across the boundary layer.

and an associated phase angle, $\phi_{pu}(\omega)$, defined by $\Phi_{pu}(\omega) = |\Phi_{pu}(\omega)| e^{j\phi_{pu}(\omega)}$, such that a negative phase indicates that the velocity lags the pressure. Frequency smoothing and phase unwrapping were applied to the computed cross-spectral results (Snarski 1993).

The coherence functions between the fluctuating wall pressure and the turbulent streamwise velocity at various wall-normal positions immediately above the pressure transducer are shown in figure 6. Although the results at only six of the nine wall-normal positions in the boundary layer are included in the figure for clarity, the remaining positions reinforce all trends reported. Near the wall ($y^+ \leqslant 28$), the coherence functions exhibit a double-humped structure with a peak located at $\omega\delta^*/U_\infty \approx 0.23$ and a band of elevated coherence in the range $\omega\delta^*/U_\infty \approx 1$ to 3 (at $y^+ = 14$, a distinct peak exists at $\omega\delta^*/U_\infty \approx 1.22$), suggesting that contributions to the wall pressure from the near-wall region result from two primary flow disturbances. This bimodal distribution of energy near the wall is consistent with the double-humped character of the first-moment velocity spectrum at $y^+ = 14$ in figure 5, except that the low-frequency peak in the velocity spectrum occurs at a slightly larger frequency of $\omega\delta^*/U_\infty \approx 0.35$. Because a similar bimodal distribution of coherent energy near the wall ($y^+ = 91$) is also apparent in the flat-plate pressure–velocity measurements of Wilczynski & Casarella (1992), the two-scale character of the near-wall pressure contributions is apparently a characteristic of all wall-bounded flows. Wietrzak & Lueptow (1994) also found elevated coherence levels at nearly identical frequencies to those found here from simultaneous measurements of the wall shear stress and the streamwise velocity near the wall in a cylindrical boundary layer ($Re_\theta = 3050$, $\delta/a = 5.7$).

With increased distance of the velocity probe from the wall, an overall decrease in

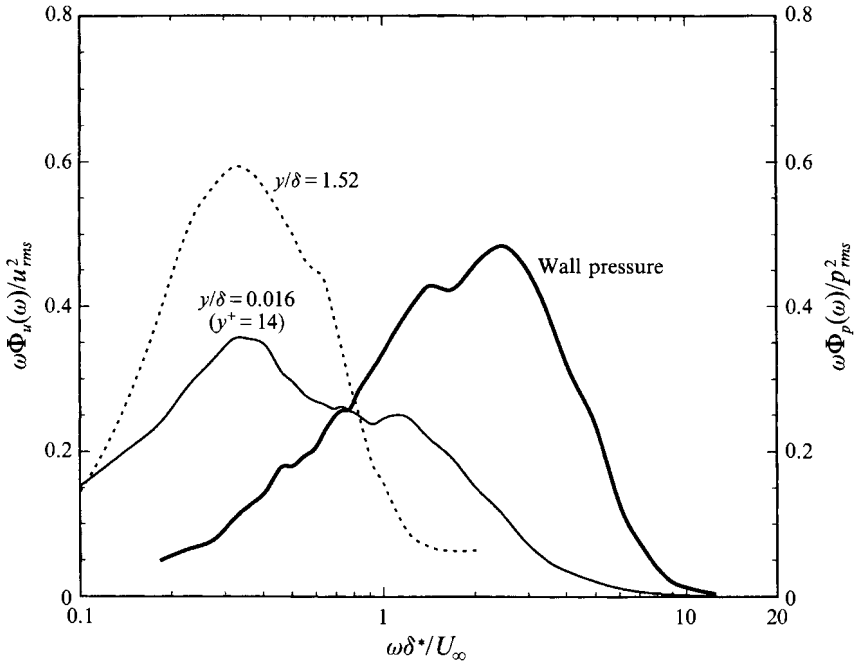

FIGURE 7. First-moment spectral density of the streamwise velocity at $y/\delta = 1.52$ and 0.016 ($y^+ = 14$) and the wall pressure. Spectral magnitudes at $y/\delta = 1.52$ are corrected to reflect unit area.

coherence levels occurs at all frequencies out to a wall-normal position of $y/\delta = 0.76$. This overall decrease in the coherent energy levels is expected since the effect of turbulent source contributions on the wall pressure varies inversely with distance from the wall. With a further increase in probe distance beyond $y/\delta = 0.76$, however, the low-frequency coherence levels near $\omega\delta^*/U_\infty = 0.23$ (the frequency at which peaks were present in the coherence functions near the wall) increase again, reaching a local maximum in the turbulent/potential flow interface at $y/\delta = 1.52$. A similar effect was observed in the first-moment velocity spectral results in figure 5, in which the spectra at $y^+ = 14$ and $y/\delta = 1.52$ both exhibit a low-frequency peak at $\omega\delta^*/U_\infty \approx 0.35$. These normalized first-moment velocity spectra are replotted in figure 7 along with the normalized first-moment wall pressure spectrum. Although the low-frequency spectral peaks appear at slightly different frequencies in figures 6 and 7, in each figure, they occur at identical frequencies for $y^+ = 14$ and $y/\delta = 1.52$. Because the peak in the velocity spectrum at $y/\delta = 1.52$ is associated with the organized irrotational motion of the turbulent/potential-flow interface, the source of the low-frequency coherence outside of the boundary layer and, therefore, near the wall is apparently the large-scale outer flow structures.

A qualitatively similar wall-normal distribution of low-frequency coherent energy to that shown in figure 6 is apparent in the flat-plate boundary layer measurements of Wilczynski & Casarella (1992) near $\omega\delta^*/U_\infty \approx 0.2$. Although the flat-plate measurements of Russell & Farabee (1991) did not extend close enough to the wall to reveal elevated low-frequency coherence near the wall, they did indicate a local maximum in low-frequency coherence near $\omega\delta^*/U_\infty \approx 0.2$ at $y/\delta = 1.5$, similar to that found in this study. This suggests that the overall behaviour of the large-scale structure is qualitatively similar in the cylindrical and flat-plate boundary layers, at least for the

moderate transverse curvature examined here. If low-frequency peaks in the first-moment spectral density of the wall shear stress and streamwise velocity in a flat-plate boundary layer are related to the statistically periodic phenomenon of bursting, as suggested by Strickland & Simpson (1975), these results provide further evidence that the burst–sweep cycle is linked to the large-scale motion in the boundary layer. The overall shift of coherent energy to lower frequencies in figure 6 with increasing distance from the wall is largely a result of the pressure-transducer/hot-wire separation distance acting as a low-pass filter, allowing only eddies with a scale larger than the distance to the wall to be correlated.

The high-frequency coherent energy peak at $\omega\delta^*/U_\infty = 1.22$ in figure 6 at $y^+ = 14$ occurs at the same frequency as the high-frequency hump in the first-moment velocity spectrum at $y^+ = 14$ in figure 7. Of greater significance, however, is that the band of coherent energy in the range $\omega\delta^*/U_\infty = 1$ to 3 near the wall in figure 6, corresponds to the peak in the first-moment spectral density of the wall pressure in figure 7 at $\omega\delta^*/U_\infty \approx 2.3$. Because a very large portion of the total r.m.s. wall pressure energy results from large-amplitude wall pressure fluctuations, presumably generated by near-wall flow structures (Schewe 1983; Karangelen & Casarella 1991), the peak in the normalized wall pressure spectrum and, hence, the high-frequency coherent energy near $\omega\delta^*/U_\infty = 1.22$ may be associated with the turbulence-generating events near the wall. More evidence is provided for this in §3.7.

The relationships between the pressure and velocity immediately above the pressure transducer shown in figure 6 exists throughout the entire domain of the measurements. This is illustrated in figure 8 in the form of contour plots of the coherence levels, constructed over all 72 points measured in the (x, y)-plane at the low and high frequencies associated with the bimodal distribution of coherent energy. At the lower frequency of $\omega\delta^*/U_\infty = 0.23$ in figure 8(*a*), the elevated coherence observed both near the wall and in the turbulent/potential flow interface exists in the form of two bands of high coherence along the entire streamwise extent of the measurement domain, with a resulting band of very low coherence between them. Although the high-coherence band in the outer part of the flow dips to zero near $x/\delta \approx 0.1$, the overall pattern of low-frequency coherence throughout the domain of the measurements suggests a large-scale flow structure with dynamical significance throughout the boundary layer. If the structure takes the form of a large rotating vortex, as has been suggested for the large-scale structure in flat-plate boundary layers (Willmarth & Wooldridge 1963; Willmarth 1975*a*; Fiedler 1986; Kobashi & Ichijo 1986), a coherence field similar to that observed in figure 8(*a*) would emerge since the streamwise velocity fluctuations due to such a structure would be largest at the top and bottom of the structure and monotonically decrease to zero at the centre of rotation. At the higher frequency $\omega\delta^*/U_\infty = 1.22$ in figure 8(*b*), the elevated coherence levels are concentrated in the inner region ($y/\delta \leqslant 0.2$) with a streamwise extent of about 1.2δ, consistent with the spatial characteristics of the near-wall turbulence-generating events (e.g. quasi-streamwise vortices, Kline & Robinson 1990; Robinson 1990). The overlap of the low- and high-frequency coherence contours for $y/\delta < 0.2$ in figures 8(*a*) and 8(*b*) illustrates the streamwise extent of the bimodal coherence distributions observed near the wall in figure 6 and, hence, the spatial coexistence of the two characteristic flow scales near the wall. The streamwise persistence of the small-scale disturbance in figure 8(*b*) may be an indication of the coupling or interdependence between the large- and small-scale motions.

Further insight into the character of both the low- and high-frequency disturbances can be obtained by examining the phase between the wall pressure and the streamwise

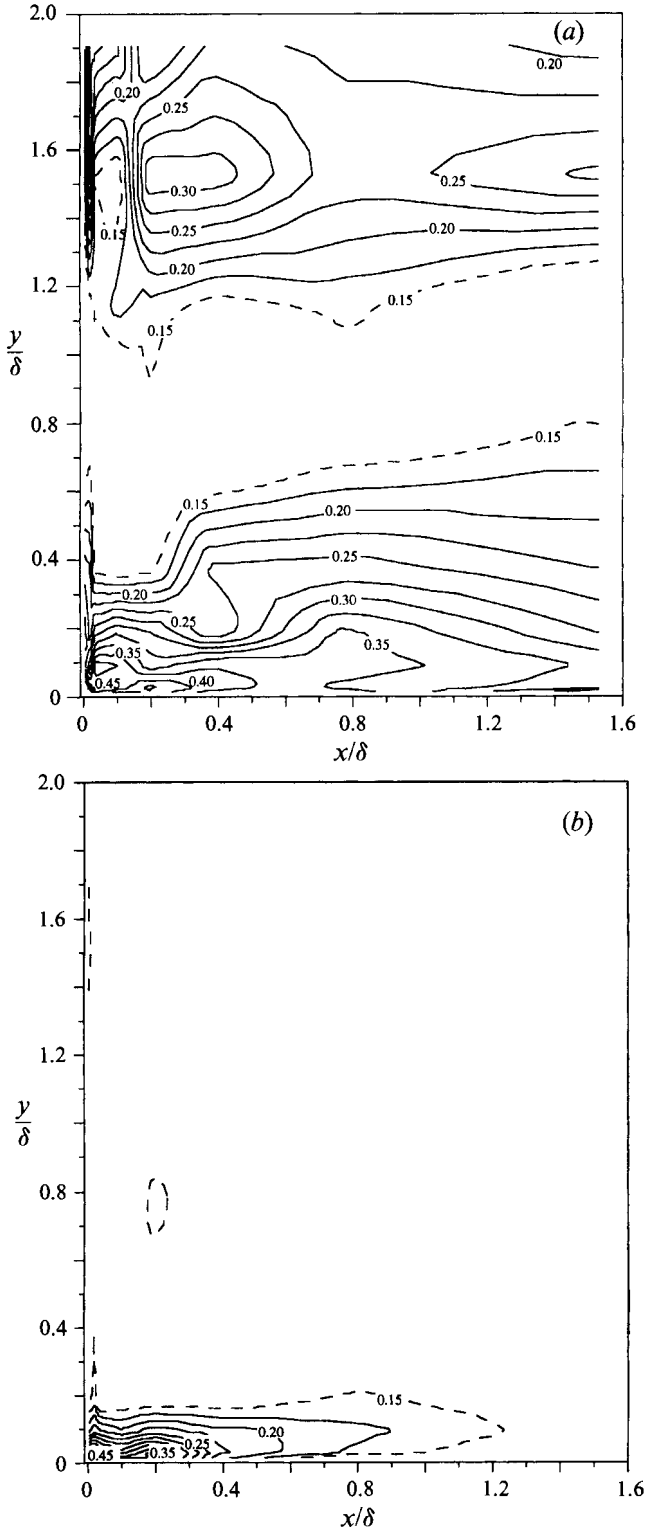

FIGURE 8. Contour plot of coherence between the wall pressure and streamwise velocity at a single frequency in (x, y)-plane containing microphone: (*a*) $\omega\delta^*/U_\infty = 0.23$ and (*b*) $\omega\delta^*/U_\infty = 1.22$.

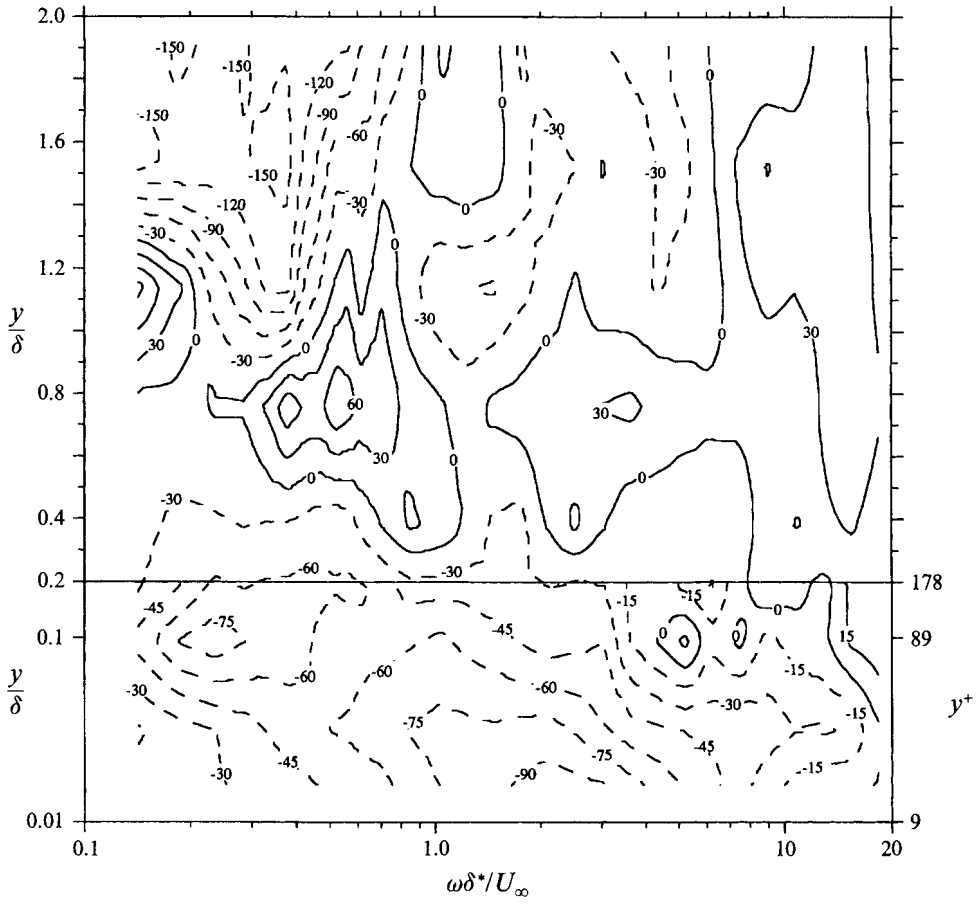

FIGURE 9. Phase between the wall pressure and streamwise velocity across the boundary layer with the hot-wire probe directly above the pressure transducer ($x = 0$). Negative phase indicates that the velocity lags the pressure.

velocity immediately above the pressure transducer, as shown in figure 9 in the form of a contour plot of $\phi_{pu}(\omega, y)$. At frequencies corresponding to the low-frequency coherence near $\omega\delta^*/U_\infty \approx 0.23$, the phase decreases monotonically as the wall is approached from $-150°$ at the farthest measurements from the wall to 0° in the region $y/\delta = 0.6$–0.8. With a further decrease in distance to the wall, the phase becomes negative again, with a local minimum of approximately $-75°$ near $y/\delta \approx 0.1$. This variation in low-frequency phase from the potential flow to the wall appears to confirm the existence of a large-scale outer structure with dynamical significance throughout the entire boundary layer, yet reveals a multilayered character of the large-scale structure not entirely predictable from a single rotating vortex (e.g. Willmarth & Wooldridge 1963; Willmarth 1975*a*; Kobashi & Ichijo 1986). At higher frequencies corresponding to the broadband concentration of coherent energy in the range $\omega\delta^*/U_\infty = 1$ to 3 near the wall, the phase varies in the range $\pm 30°$ for $y/\delta > 0.5$, but decreases monotonically below this point, reaching a value of $-90°$ at the closest position to the wall ($y^+ = 14$, $y/\delta = 0.016$). Because the $-90°$ phase near the wall is consistent with the relationship between conditionally sampled large-amplitude wall pressure peaks and velocity shear layers in the near-wall region, to be discussed in §3.7,

these results provide additional support to the idea that the high-frequency coherent energy is associated with the turbulence-generating events near the wall. Although qualitatively similar phase relationships could be deduced from pressure-velocity correlation measurements performed in flat-plate boundary layers (Willmarth & Wooldridge 1963; Panton *et al.* 1980; Kobashi & Ichijo 1986), phase results have not been reported. Consequently, quantitative effects of transverse curvature are difficult to deduce.

3.6. *Pressure–velocity cross-correlations*

Information concerning the spatial–temporal relationships between the wall pressure and streamwise velocity can be obtained from the cross-correlation coefficient. Such correlations have been used in flat-plate boundary layers to study both the turbulent sources of the wall pressure and the structure of the turbulent boundary layer (Willmarth & Wooldridge 1963; Willmarth & Tu 1967; Panton *et al.* 1980; Kobashi & Ichijo 1986). The correlation coefficient was computed using Fourier transform methods according to

$$\rho_{pu}(\tau; x, y) \equiv \frac{\langle p(t; 0, 0)\, u(t+\tau; x, y)\rangle}{p_{rms}\, u_{rms}} = \frac{1}{p_{rms}\, u_{rms}} \int_{-\infty}^{\infty} S_{pu}(f; x, y)\, \mathrm{e}^{j2\pi f\tau}\, \mathrm{d}f, \qquad (2)$$

where $S_{pu}(f) = \Phi_{pu}(f)/2$ is the double-sided cross-spectrum defined for $-\infty < f < \infty$. The results were computed using 100% zero padding to obtain the linear rather than circular correlation (Bendat & Piersol 1986).

The pressure–velocity correlation measurements in the (x, y)-plane containing the microphone are summarized in figure 10 by means of a contour plot constructed from the correlation magnitude at zero time delay for all 72 points in the plane. Because the cross-correlation is the integral of the cross-spectrum over frequency, the correlation contours incorporate the coherence and phase information at all frequencies and all positions in the plane into a single plot. Since the isocontours are constructed at a single time delay ($\tau = 0$), they depict an instant in time and thus represent a 'snapshot' of the average eddy structure throughout the boundary layer that contributes to the fluctuating wall pressure. Because Taylor's frozen field hypothesis $\tau = x/U_c$ is only valid for spatial intervals that are short relative to the distance over which the eddies decay, the isocontours provide insight into the character of the large-scale structure which has a decay length much greater than the spatial extent of the measurements. The sign of the correlation in the isocontour plot is a direct indication of the average sign of the product of the pressure and velocity at $\tau = 0$.

Near the wall, a series of negative contours (-0.07 to -0.01) exist at an angle of approximately 18° to the wall. Willmarth & Wooldridge (1963) found similar negative contours from pressure–velocity correlation measurements in a flat-plate boundary layer. The angle of these contours suggests that they are related either to near-wall shear layers or large-scale coherent structures termed 'backs', both of which are typically inclined at 12°–30° to the wall in flat-plate boundary layers (Brown & Thomas 1977; Thomas & Bull 1983; Kline & Robinson 1990; Robinson *et al.* 1990). A similar angle of inclination was deduced from simultaneous wall shear stress and streamwise velocity measurements in a cylindrical boundary layer (Wietrzak & Lueptow 1994). The isocorrelation contours also reveal a band of positive correlation that extends out from the wall past the edge of the boundary layer at an angle of approximately 45°, suggesting the presence of a large-scale flow structure inclined to the wall. Bull & Dekkers (1993) deduced a similar angle of inclination for large-scale crossflow fronts of low-speed ($u < 0$) fluid for cylindrical boundary layers with $\delta/a = 26$ to 42. Because

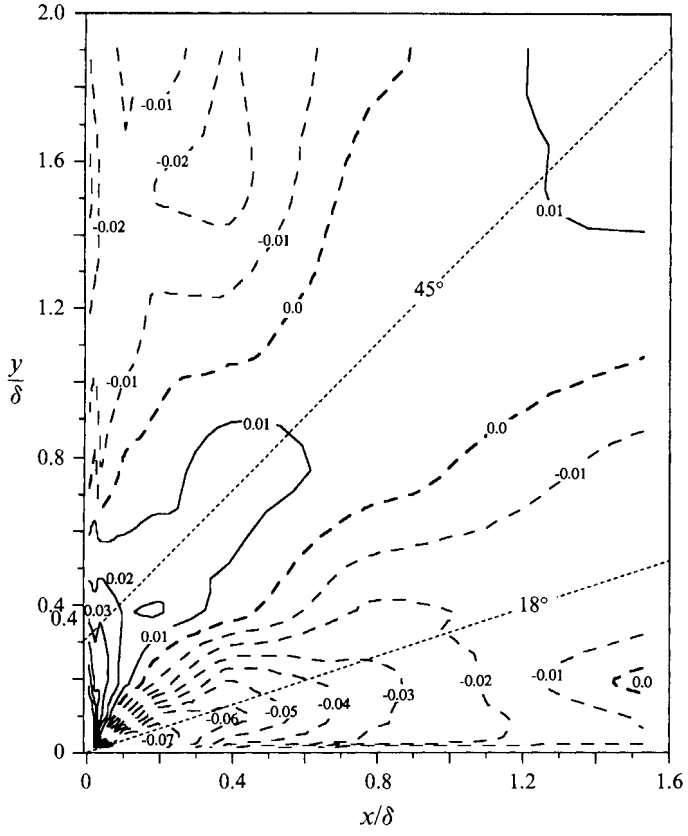

FIGURE 10. Contour plot of cross-correlation between the wall pressure and streamwise velocity for zero time delay ($\tau = 0$) in (x, y)-plane containing microphone.

correlation contours in flat-plate boundary layers have not revealed similar 45° inclined contours (Willmarth & Wooldridge 1963), the 45° band of positive correlation may be related to these crossflow low-speed fronts. However, 45° angles of inclination for large-scale vortical structures have been identified using other techniques in flat-plate boundary layers (Head & Bandyopadhyay 1981; Fiedler 1986; Robinson 1990) and in a simulated channel flow (Moin & Kim 1985), suggesting that the structure may not be peculiar to the cylindrical boundary layer.

In fact, if the band of positive correlation in figure 10 is instead assumed to be high-speed fluid ($u > 0$), a conceptual model can be formulated for the large-scale structure that is entirely consistent with the correlation contours in figure 10 as well as compatible with models proposed for the large-scale structure in flat-plate boundary layers. The conceptual model for the large-scale structure is shown in figure 11 in a reference frame with the mean velocity profile removed or one moving approximately with the structure (or $\sim 0.83U_\infty$ as will be deduced shortly). To emphasize the consistency between the model and the measured pressure–velocity correlations, an overlay of a frame corresponding to the contours in figure 10 is also included in figure 11. Because positive correlations are assumed to represent high-speed fluid ($u > 0$), the model implicitly assumes that the average pressure is positive at $\tau = 0$.

The conceptual model consists of a large inclined vortex that rotates in the direction of the mean shear with its trailing face at an angle of 45° to the wall and its leading face

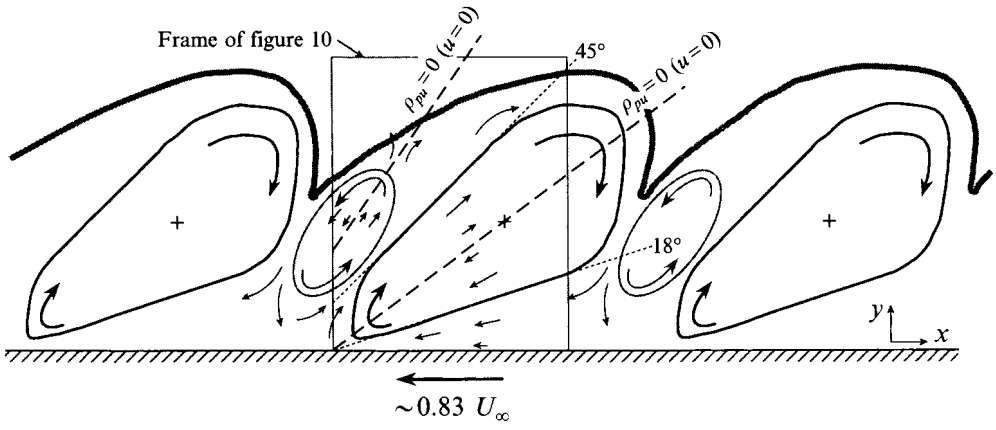

FIGURE 11. Conceptual model of large-scale boundary layer structure based on zero time delay correlations between the fluctuating wall pressure and streamwise velocities in frame of reference with mean velocity profile removed.

at an angle of 18° to the wall and an average height of approximately 1.5δ. As discussed in §3.5, since the streamwise velocity fluctuations due to a rotating vortex structure would be largest at the top and bottom and monotonically decrease to zero at the centre of rotation, the model qualitatively predicts the behaviour of the low-frequency energy in the pressure–velocity coherence in figure 8(*a*). Because the low-frequency spectral humps near the wall and in the turbulent/potential-flow interface in figures 5 and 6 disappear at the intermediate measurement points, the intensity of the streamwise velocity fluctuations due to the large-scale structure are apparently below the stochastic background except very near the upper and lower periphery. The shear created between the upstream and downstream faces of two adjacent large-scale vortices induces a secondary vortex of opposite rotation between them. By having these counter-rotating vortices overlap, the variation in low-frequency phase between the pressure and streamwise velocity with distance from the wall would be multilayered in character, similar to the low-frequency phase results in figure 9. Along the bisectors of these counter-rotating vortices, shown as bold dashed lines in the figure at angles of approximately 35° and 55° to the wall, the streamwise velocity is zero; hence, the vortices correspond to the zero-correlation lines in figure 10. Because the velocity changes sign across each of these lines, but in opposite directions, the lines represent shear layers of opposite sign in the flow. The lines at 18° and 45°, on the other hand, represent the loci of maximum negative or positive streamwise velocity, respectively.

The form for the large-scale structure proposed here is compatible with models proposed for the large-scale structure in flat-plate boundary layers (Willmarth 1975*a*; Thomas & Bull 1983; Fiedler 1986; Kobashi & Ichijo 1990) as well as with most of the observed large-scale structural features of flat-plate boundary layers (e.g. δ-scale backs, pressure pockets, inward and outward interactions). This suggests that the large-scale motion is qualitatively similar in the cylindrical and flat-plate boundary layers, at least for the moderate transverse curvature examined here. The crossflow fronts of low-speed fluid observed by Bull & Dekkers (1993) may have been a byproduct of the larger transverse curvature ratios used in their experiments.

Further insight into the character of the large-scale structure can be obtained by examining the local convection velocities of the space–time pressure-velocity correlations, as shown in figure 12 for several wall-normal positions of the hot-wire

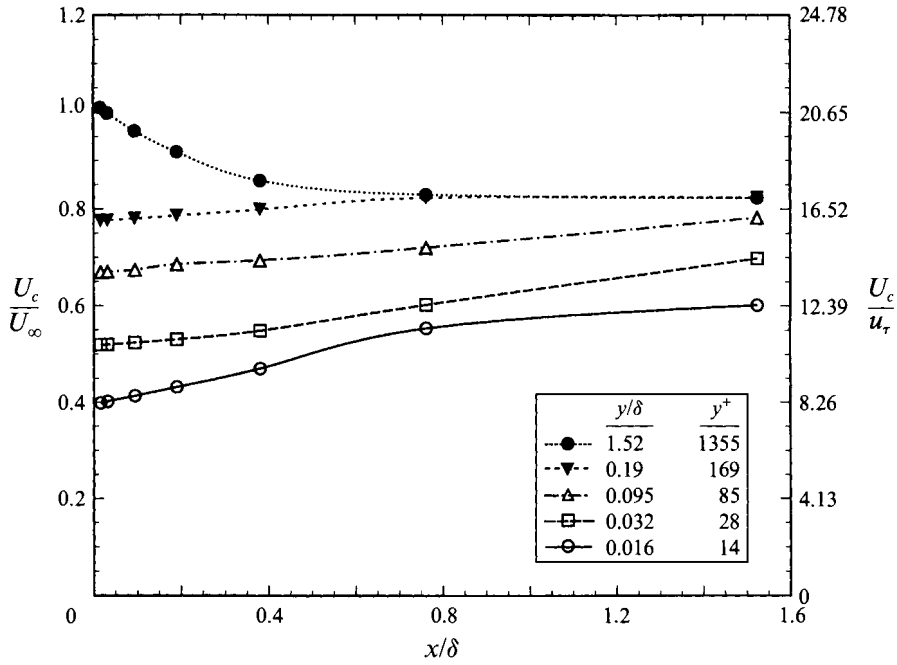

FIGURE 12. Local convection velocity of the correlation between the wall pressure and streamwise velocity at various wall-normal positions of the hot wire. Convection velocities computed from the locus of maximum correlation amplitudes in the (x,τ)-plane.

probe. The convection velocities U_c were computed from the time shifts τ_c associated with the locus of maximum correlation amplitudes in the (x,τ)-plane according to $U_c = x/\tau_c$ (Hinze 1975). Within the inner region $y/\delta \leqslant 0.19$, the local convection velocities show an increase with increased streamwise separation, due to the decay of smaller, slower eddies near the wall (Willmarth & Wooldridge 1962; Willmarth & Yang 1970). Because these smaller scales near the wall decay within a distance of $x/\delta \approx 1.2$ according to figure 8(*b*), the convection velocities at $x/\delta \approx 1.5$ in figure 12 reflect the velocity of the (remaining) large-scale, pressure-producing structure. Outside the boundary layer ($y/\delta = 1.52$), the local convection velocities show a decrease with increased streamwise separation, presumably due to the loss of momentum of the fluid at the turbulent/potential interface to the boundary layer. At large x, the convection velocities at both $y/\delta = 1.52$ and 0.19 asymptotically approach the value of $0.83U_\infty$, consistent with the mean convection velocity for the large-scale pressure-producing structure measured with streamwise-separated pressure transducers in both cylindrical (Willmarth & Yang 1970) and flat-plate boundary layers (Willmarth & Wooldridge 1962). Using this mean convection velocity, the characteristic frequency $\omega\delta^*/U_\infty \approx 0.23$ of the large-scale structure deduced from the coherence results in figure 6 corresponds to a convected wavelength of approximately 4δ–consistent with that deduced by Laufer (1972) for the average wavelength of the wavy outer interface in a flat-plate boundary layer. Because the correlation results in figure 10 contain frequency information in the band $0.13 \leqslant \omega\delta^*/U_\infty \leqslant 12.5$, however, a smaller wavelength of 2.2δ was required for the convected spatial period of the large-scale structure in figure 11. That the limiting convection velocities associated with the large-scale structure near the wall are less than those elsewhere in the boundary layer may be an indication that the large-scale structure (primary and/or secondary vortices in figure 11) is stretched in the

streamwise direction near the wall owing to the large mean velocity gradients present there. Kobashi & Ichijo (1990) suggested that this type of stretching of the large-scale structure near the wall was responsible for the formation of near-wall vortex structures and bursts in a flat-plate boundary layer. More insight into the relationship between the large-scale flow structures and the near-wall turbulence-generating events is provided in the next section by examining the character of the small-scale structure near the wall.

3.7. *Conditional sampling of wall pressure and streamwise velocity events*

The relationship between the fluctuating wall pressure and the streamwise velocities in the near-wall region was investigated using conditional sampling. These conditional sampling procedures utilize various detection schemes to identify a repeated pattern, salient feature, or 'event' in a signal. Once the detection times for the events are identified, conditional averages of the event signature can be constructed and related to conditional averages of a secondary signal computed at the same detection times. Here, the technique is used to determine if a relationship exists between large-amplitude short-duration wall pressure fluctuations and layers of high shear near the wall – both of which are believed to be associated with turbulence production (i.e. the burst–sweep cycle) in flat-plate boundary layers (Schewe 1983; Thomas & Bull 1983; Kobashi & Ichijo 1986; Johansson *et al.* 1987; Haritonidis *et al.* 1990).

To deduce the character of the wall pressure signal generated by the passage of a high-shear layer, a variable interval time averaging (VITA) detection scheme (Blackwelder & Kaplan 1976; Johansson & Alfredsson 1982) was used to detect sharply changing streamwise velocities by examining the magnitude of the short-time variance of the velocity signal. Both accelerating velocity events ($\partial u/\partial t > 0$) and decelerating velocity events ($\partial u/\partial t < 0$) were distinguished. Because VITA-detected events depend on both the threshold level κ and the averaging time T, these detection parameters should be chosen to correspond closely with the time scales of the flow structure under investigation. Since a threshold level $\kappa = 1$ has been used extensively in flat-plate boundary layers to detect bursts and determine the bursting frequency (Blackwelder & Kaplan 1976; Johansson & Alfredsson 1982; Willmarth & Sharma 1984; Yuan & Mokhtarzadeh-Dehghan 1994), a value of $\kappa = 1$ was also used here. For the averaging time, a value corresponding to $T^+ = Tu_\tau^2/\nu = 18.4$ was used since it produced the highest frequency of occurrence of accelerating events at $y^+ = 14$ – the most probable event duration for events related to the burst–sweep cycle (Johansson & Alfredsson 1982). This optimal averaging time or burst duration of $\Delta T_b^+ = 18.4$ and the associated bursting period (deduced from the average time between events) of $\bar{T}_b^+ = 211$ are similar to other measurements in cylindrical (Lueptow & Haritonidis 1987) and flat-plate boundary layers (Lu & Willmarth 1973; Johansson & Alfredsson 1982; Willmarth & Sharma 1984; Johansson *et al.* 1987; Shah & Antonia 1989).

To deduce the character of the streamwise velocity signals during the occurrence of large-amplitude wall pressure fluctuations, a pressure-peak detection scheme (Johansson *et al.* 1987; Haritonidis *et al.* 1990; Dinkelacker 1990) was utilized. Both positive ($p \geqslant \kappa p_{rms}$) and negative ($p \leqslant -\kappa p_{rms}$) events were identified. If the pressure-peak and VITA detection schemes are to be used to study the relationship between large-amplitude wall pressure events and bursting events, the event time scales from the two detection schemes should be similar (Johansson *et al.* 1987; Yuan & Mokhtarzadeh-Dehghan 1994). For pressure-peak threshold levels of $\kappa = 2$–3, the average time between and duration of positive or negative pressure peaks are $\bar{T}^+ = 138$–583 and $\Delta T^+ = 15.7$–13.3, respectively – comparable to the time scales

of the VITA-detected bursting events in the near-wall region (e.g. $\bar{T}^+ = 211$ and $\Delta T^+ = 18.4$). These time scales are also consistent with the characteristics of pressure peaks of similar magnitude in flat-plate boundary layers believed to be associated with the bursting process in the near-wall region (Schewe 1983; Johansson *et al.* 1987; Karangelen *et al.* 1991). At all threshold levels examined, negative pressure peak events occur slightly more frequently and have a slightly shorter duration than positive pressure peak events. To facilitate comparison with measurements in flat-plate boundary layers, a threshold level of $\kappa = 2.5$ is used for the conditionally averaged results.

The conditionally sampled pressure and velocity signatures obtained with the hot-wire probe immediately above the pressure transducer ($x^+ = 0$) are shown in figure 13. In figure 13(*a*), the velocity signatures at each wall-normal location are obtained by conditionally sampling the velocity signals at the detection times established by the detected pressure peaks. The positive or negative pressure signatures are nearly identical at each y^+, although those at $y^+ = 14$ are slightly affected by the presence of the hot-wire probe (see §2.3). In figure 13(*b*), the pressure signals are conditionally sampled at the detection times set by the VITA technique applied to u (or VITA-on-u) at the various distances from the wall. The conditional averages are non-dimensionalized by the respective r.m.s. values. For the pressure-peak detection results, the pressure signal is also divided by the threshold κ. In all the figures, the trigger signal is denoted by a bold curve.

Very near the wall ($y^+ = 14$), the conditionally averaged pressure and velocity signatures obtained from the pressure peak and VITA-on-u detection schemes are qualitatively similar, as is evident by comparing figures 13(*a*) and 13(*b*). Detected positive large-amplitude wall pressure peaks are associated with local increases or accelerations in streamwise velocity, while streamwise velocity accelerations detected using VITA are associated with positive peaks in the wall pressure. Similarly, detected negative large-amplitude pressure peaks are associated with local decreases in streamwise velocity, while VITA-detected decelerations in streamwise velocity are associated with negative peaks in the wall pressure. This qualitative similarity or reciprocity between the VITA-on-u and pressure-peak detection results illustrates a bidirectional relationship or coupling between large-amplitude wall pressure fluctuations and the rate-of-change of streamwise velocity near the wall. The coupling between decelerations and negative pressure peaks appears weaker than that for the positive pressure peaks and accelerations, possibly because the detection parameters were optimized for accelerating VITA events. Because a $-90°$ phase relationship exists between the conditionally averaged pressure peak and streamwise velocity signatures, these results are consistent with the $-90°$ phase of the pressure–velocity cross-spectra near the wall ($y^+ = 14$, $y/\delta = 0.016$) at high frequencies ($\omega\delta^*/U_\infty \approx 1$ to 3) in figure 9.

The bidirectional relationship near the wall is further demonstrated in figure 14, where for both detection schemes the amplitude of the pressure is plotted against the temporal derivative of the streamwise velocity ($\partial u/\partial t$) at $y^+ = 14$ for each event at the time of detection. The gap in the data points in figure 14(*a*) is a result of the pressure threshold used for the pressure-peak detection scheme. Clearly, a distinct correlation exists between p and $\partial u/\partial t$ for both detection schemes, as evidenced by the concentration of points along a band through the first and third quadrants. This coupling between p and $\partial u/\partial t$ for both positive and negative peaks indicates that both types of large-amplitude wall pressure fluctuations are directly linked to flow structures in the near-wall region and that both are important to the physics of the near-wall flow. Positive pressure peaks are produced by local accelerations of fluid ($\partial u/\partial t > 0$)

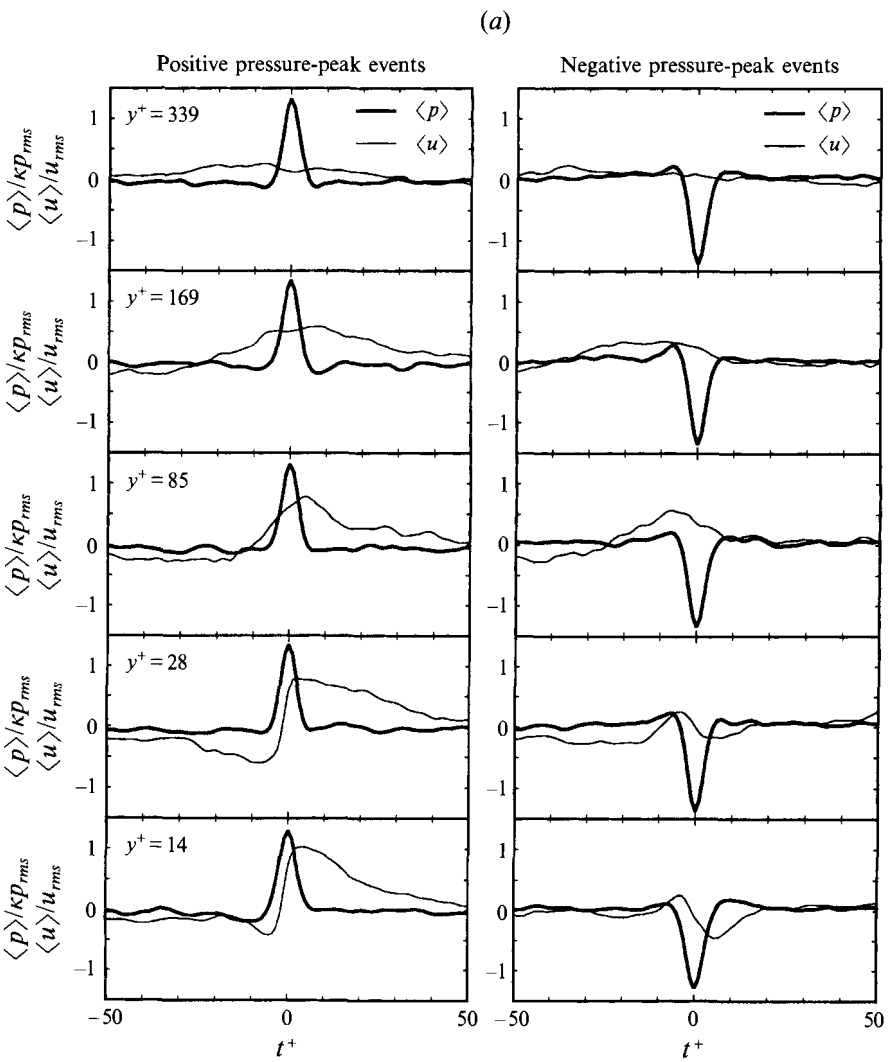

FIGURE 13(*a*). For caption see facing page.

in the near-wall region and are thus associated with shear layer structures presumably related to bursting. Negative pressure peaks, on the other hand, are produced by local decelerations of fluid ($\partial u/\partial t < 0$) near the wall. Although the flat-plate boundary layer measurements of Johansson *et al.* (1987) and Haritonidis *et al.* (1990) emphasized the relationship between positive pressure peaks and accelerating VITA-on-*u* events, a relationship between negative pressure peaks and decelerating streamwise velocities is evident in both sets of measurements. In addition, a coupling between both positive and negative pressure peaks and the near-wall flow was reported for conditional sampling measurements in a turbulent pipe flow (Dinkelacker 1990). This indicates that the coupling between both positive and negative pressure peaks and flow structures in the near-wall region is a general characteristic of all wall-bounded flows.

Evidence linking these near-wall flow structures and the large-scale motion in the boundary layer is provided by considering the burst frequency, or frequency of occurrence, deduced from the average time between either VITA-on-*u* or pressure-

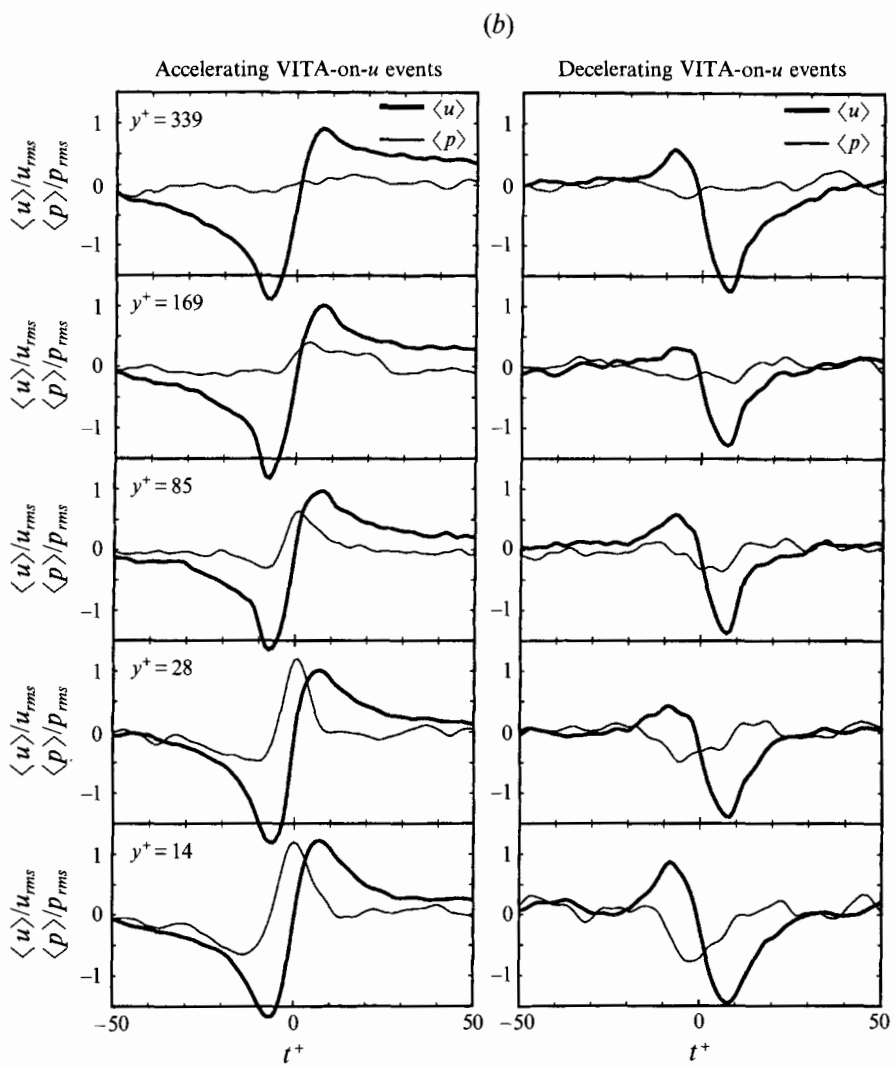

FIGURE 13. Conditionally averaged wall pressure and streamwise velocity signatures at various y^+ positions of the hot wire: (*a*) detection of positive (left) and negative (right) pressure-peak events ($\kappa = 2.5$); (*b*) VITA detection of accelerating (left) and decelerating (right) events in u ($\kappa = 1.0$, $T^+ = 18.4$). Bold curves denote trigger signal.

peak events. Scaled on outer variables, the frequencies associated with the VITA burst period of $\bar{T}_b^+ = 211$ and the pressure-peak period of $\bar{T}^+ = 138$–583 are $\omega\delta^*/U_\infty = 0.23$ and $\omega\delta^*/U_\infty = 0.08$–$0.35$, respectively. Because these frequencies are consistent with the low-frequency concentration of energy observed both near the wall and in the turbulent/potential flow interface in figures 5 and 6, the low-frequency humps are apparently associated with the statistically periodic phenomenon of bursting as originally suggested by Strickland & Simpson (1975) for the first-moment spectral density of the wall shear in a flat-plate boundary layer. More importantly, however, if this low-frequency energy is associated with the characteristic large-scale structure in the boundary layer as previously suggested, this result implies that the burst–sweep cycle responsible for the turbulence production near the wall is linked to the large-scale motion in the boundary layer. Kobashi & Ichijo (1990) suggested that

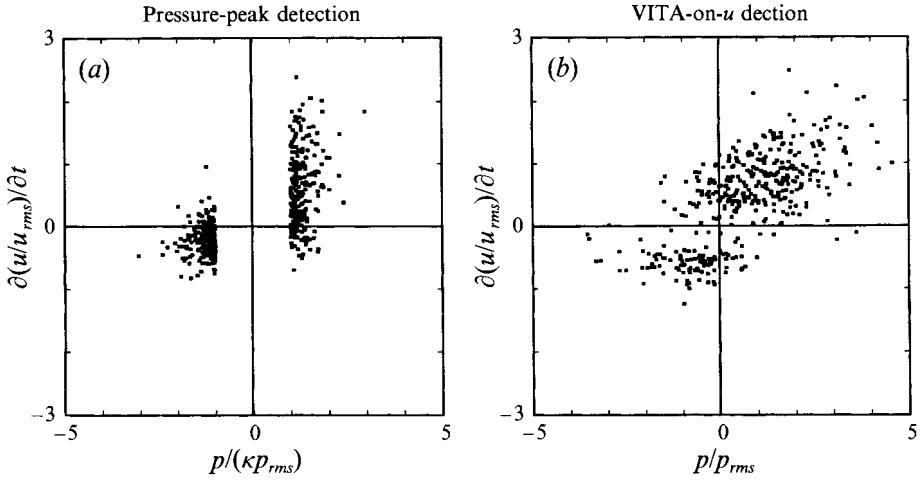

FIGURE 14. Temporal derivative of streamwise velocity at $y^+ = 14$ versus amplitude of wall pressure at time of detection. (*a*) pressure-peak detection ($\kappa = 2.5$), (*b*) VITA-on-*u* detection ($\kappa = 1.0$, $T^+ = 18.4$).

a stretching of the large-scale structure near the wall was responsible for bursts in flat-plate boundary layers. If such a stretching occurs in the conceptual model for the large-scale structure in figure 11, a direct mechanism for the near-wall turbulence-generating events would exist since the counter-rotating vortices are associated with shear layers of opposite sign and would thus create both accelerating and decelerating VITA events (e.g. rapid changes in u) near the wall. Because the VITA bursting frequency has been found to be nearly constant across the entire boundary layer (Lu & Willmarth 1973; Hinze 1975; Johansson & Alfredsson 1982), this link between the large- and small-scale motions may explain why the low-frequency spectral humps occur at the same frequencies near the wall and at the edge of the layer in figures 5 and 6 even though the convection velocity of the large-scale structure at the two points is slightly different (i.e. figure 12). Thomas & Bull (1983) also found a link between the large- and small-scale motions in a flat-plate boundary layer by conditional sampling the low-frequency portion of the wall pressure signal on the large-amplitude wall pressure peaks but concluded that the large-scale structure was not directly responsible for the bursting process near the wall.

Also of interest are the frequencies associated with the event time durations. Scaled on outer variables, the frequencies corresponding to the optimal VITA averaging time or burst duration of $\Delta T_b^+ = 18.4$ and the maximum pressure event duration of $\Delta T^+ = 15.7$ are $\omega\delta^*/U_\infty = 2.6$ and 3.1, respectively. These frequencies, associated with the characteristic time scale of the near-wall turbulence-generating flow structures, are commensurate with the frequencies at which a high-frequency concentration of energy occurred in the pressure–velocity coherence results near the wall in figure 6 as well as with the frequencies at which the peak energies occurred in the first-moment pressure spectrum in figure 7. As such, this result provides support for the assertion that the source of the high-frequency coherence near the wall (in the band $1 < \omega\delta^*/U_\infty < 3$) is the turbulence-generating events related to the burst–sweep cycle and that the peak in the first-moment spectral density of the wall pressure (at $\omega\delta^*/U_\infty = 2.3$) is related to the large-amplitude wall pressure fluctuations associated with turbulence production near the wall.

For either detection scheme in figure 13, the relationship between the conditionally averaged pressure and velocities weakens considerably with increasing y. The bidirectional relationship between positive large-amplitude wall pressure peaks and shear layer structures observed at $y^+ = 14$, although nearly as strong at $y^+ = 28$, diminishes rapidly with a further increase in y such that by $y^+ = 169$, the relationship is nearly gone. A similar trend was found for the positive large-amplitude wall pressure peaks in a flat-plate boundary layer (Johansson *et al.* 1987). Because the relationship between negative pressures and decelerating velocities in figure 13 is not as strong at $y^+ = 14$, the relationship decays even more rapidly with y, although this may again be because the detection parameters were optimized for accelerating VITA events. This decoupling of the pressure peaks from $\partial u/\partial t$ with increased y causes the correlation between pressure peaks and $\partial u/\partial t$ present at $y^+ = 14$ in figure 14 to disappear such that the distinct bands become a random distribution of points in all four quadrants for both detection schemes. These results indicate that the flow disturbances responsible for the high-frequency large-amplitude wall pressure peaks are concentrated primarily within the buffer layer ($y^+ \leqslant 28$), although they are also present throughout the near-wall region ($y^+ < 100$) – consistent with the character of the turbulence-generating events in a flat-plate boundary layer.

The convective behaviour of the near-wall ($y^+ = 14$, 28) flow structures responsible for the large-amplitude wall pressure fluctuations was deduced by examining the conditionally sampled pressure and velocity signatures with various streamwise separation distances between the hot wire and pressure transducer. As the streamwise separation between the pressure transducer and the hot-wire probe increases, no appreciable change occurs in the magnitude or duration (width) of the shear layer pattern until a streamwise separation of $x^+ = 339$ is reached, indicating that the pressure-producing structures in the near-wall flow remain fairly coherent over this distance. Between $x^+ = 677$ ($x/\delta = 0.76$) and $x^+ = 1355$ ($x/\delta = 1.52$), the correlated pattern disappears altogether, indicating that the near-wall structure responsible for the large-amplitude wall pressure fluctuations remains intact for a streamwise extent of $x^+ \sim 1000$ ($x/\delta \sim 1$). This distance is comparable to that for the characteristic pressure pattern in a flat-plate boundary layer using streamwise-separated pressure transducers (Schewe 1983) and is consistent with the convective behaviour of the near-wall quasi-streamwise vortex structure believed to be associated with the burst–sweep cycle in a flat-plate boundary layer (Kline & Robinson 1990; Robinson 1990). This streamwise extent is also consistent with the streamwise extent over which high-frequency coherence was concentrated in figure 8(*b*), providing additional support for the idea that the high-frequency coherence is associated with turbulence-generating events near the wall.

The average convection velocities for the near-wall pressure-producing structure (deduced from the time shifts associated with the pressure or velocity patterns at a streamwise separation distance $x^+ = 339$) at $y^+ = 14$ and 28, respectively, are $10.9u_\tau$ and $12.7u_\tau$ for the positive-pressure/accelerating-velocity events and $9.2u_\tau$ and $10.6u_\tau$ for the negative-pressure/decelerating-velocity events – consistent with the convection velocities derived from the pressure–velocity correlation shown in figure 12. These values are also comparable to the convection velocity of $11.9u_\tau$ for the characteristic pressure pattern in a flat-plate boundary layer deduced from streamwise-separated pressure transducers (Schewe 1983). The lower convection velocity for the negative wall pressure peaks and decelerating velocity patterns observed in the present measurements has not been previously reported, and suggests that the sources for the negative pressure peaks are concentrated closer to the wall. This effect could contribute

to the weaker coupling between negative-pressure peaks and decelerating-velocity events at any given y and the more rapid decay of the negative-pressure/decelerating-velocity events with increased distance from the wall in figure 13.

4. Discussion and conclusions

The goal of this study was to determine the flow structures in the turbulent boundary layer on a cylinder in axial flow that contribute to the fluctuating pressure at the wall and, through comparison with results for flat-plate boundary layers, determine the effect of transverse curvature on the structure of boundary layer turbulence. The results indicate that two primary groups of flow disturbances contribute to the fluctuating pressure at the wall in the cylindrical boundary layer. Pressure–velocity coherence results near the wall ($y^+ = 14$) are bimodal in character, containing distinct peaks at both low and high frequencies. A similar bimodal distribution of energy was also apparent in the first-moment spectral density of the streamwise velocity at $y^+ = 14$. The low-frequency pressure–velocity coherence peak, which occurs at a frequency of $\omega\delta^*/U_\infty \approx 0.23$, is also the frequency at which a peak occurs in the coherence between the wall pressure and streamwise velocity outside of the boundary layer. This result, also evident in the first-moment streamwise velocity spectra, suggests that the source of the low-frequency coherent energy is a large-scale structure with dynamical significance across the entire boundary layer. The high-frequency peak in the pressure–velocity coherence function near the wall that occurs at a frequency of $\omega\delta^*/U_\infty \approx 1.22$ (and the associated band of coherent energy in the range $1 < \omega\delta^*/U_\infty < 3$) exists only very close to the wall ($y/\delta < 0.2$), has a streamwise extent of over δ, and has a pressure–velocity phase relationship near $-90°$ within the buffer layer. Because the relationship between large-amplitude wall pressure fluctuations and VITA-on-u events in the near-wall region exhibit the same attributes with a characteristic frequency based on an event duration of $\omega\delta^*/U_\infty \approx 2.6$ to 3.1, the source of the high-frequency energy is apparently the turbulence-generating events near the wall. A similar two-scale character has been deduced for the pressure-producing turbulence structure of flat plate boundary layers (Thomas & Bull 1983; Kobashi & Ichijo 1990).

Evidence was also provided that shows a clear link between the large-scale motion and the bursting events near the wall. The low-frequency energy in the coherence between the wall pressure and the streamwise velocity outside of the boundary layer as well as the first-moment streamwise velocity spectra occur at the same frequency within the buffer layer. Because this frequency is also consistent with the bursting frequency deduced from the average time between accelerating VITA-on-u and large-amplitude wall pressure events, the results suggest that the burst–sweep cycle is linked to the large-scale motion. Thus, the bimodal distribution of energy present in the pressure–velocity and velocity spectra at $y^+ = 14$, which indicates the presence of two characteristic frequencies near the wall, can be traced to the two characteristic time scales describing the bursting process: the time between events (the lower frequency) and the event durations (the higher frequency). Although a coupling between the large- and small-scale motions has also been found to exist in flat-plate boundary layers, the connection between the two characteristic frequencies near the wall and the two characteristic time scales associated with the bursting process has not been previously identified.

From pressure–velocity cross-correlations, a conceptual model for the large-scale structure in the boundary layer was deduced that accurately predicts the observed pressure–velocity correlation contours while providing qualitative insight into the

source of the observed pressure–velocity coherence and phase results at low frequencies. The model (figure 11) consists of (i) a primary spanwise-oriented vortex that rotates in the direction of the mean shear with its leading face at an angle of 18° to the wall and its trailing face at an angle of 45° and (ii) an induced secondary counter-rotating vortex. The model is compatible with those proposed for the large-scale structure in flat plate boundary layers (Willmarth 1975*a*; Thomas & Bull 1983; Fiedler 1986; Kobashi & Ichijo 1990) as well as with most of the observed large-scale structural features of flat-plate boundary layers (e.g. δ-scale backs, pressure pockets, inward and outward interactions). From the local convection velocities of the space–time pressure–velocity correlations, the velocities associated with the large-scale structure near the wall are less than those elsewhere in the boundary layer, suggesting that the large-scale structure (primary and/or secondary vortices) is stretched in the streamwise direction near the wall. Kobashi & Ichijo (1990) suggested that a stretching of the large-scale structure near the wall was responsible for bursts in flat-plate boundary layers. As described below, such a stretching of the large-scale structure proposed here provides a direct mechanism to couple the large- and small-scale motions in the boundary layer.

Willmarth & Yang (1970) and Willmarth *et al.* (1976) made measurements of the fluctuating wall pressure in cylindrical boundary layers with $\delta/a \approx 2$ and 4 and found that the wall pressure spectral energy was reduced at low frequencies and increased at high frequencies in the boundary layer with transverse curvature – a result used to support their conjecture that the pressure-producing eddies in the cylindrical boundary layer are smaller. Although a similar result exists for the present measurements when non-dimensionalized in the form used by Willmarth, the cylindrical and flat-plate spectra collapse if δ rather than δ^* is chosen for the length scale. However, because both δ and δ^* (as well as ν/u_τ) are functions of transverse curvature (due to the larger skin friction and, hence, fuller mean velocity profile in the cylindrical boundary layer), it is difficult to assess the true effect of transverse curvature on the wall pressure spectrum. The effect of transverse curvature on the wall pressure statistics is also difficult to deduce due to insufficient data.

Conditional sampling of the pressure and velocity signals using pressure-peak and VITA-on-u detection schemes indicates a distinct bidirectional relationship between both positive and negative large-amplitude wall pressure fluctuations and the temporal derivative of u in the near-wall region – positive pressure peaks are associated with streamwise accelerations ($\partial u/\partial t > 0$) while negative pressure peaks are associated with streamwise decelerations ($\partial u/\partial t < 0$). This suggests that both types of processes are important to the physics of the near-wall flow. Because the counter-rotating vortices in the conceptual model proposed for the large-scale structure (figure 11) introduce shear layers of opposite sign into the flow, a mechanism is provided for both accelerating and decelerating VITA events (e.g. rapid changes in u) near the wall if the large-scale structure is highly stretched and elongated close to the wall, as was suggested by the convection velocity results obtained from the space–time pressure–velocity correlations. From the conditionally sampled pressure and velocity results, the convection velocity for decelerating VITA events is less than that for the accelerating events, suggesting that the sources for the negative pressure peaks may be concentrated closer to the wall.

Although the collective body of results presented here indicates that the turbulence structure is similar in cylindrical and flat-plate boundary layers, it is necessary to note that the structure of flat-plate turbulent boundary layers is not completely understood. As a result, it is difficult to conclude in some instances whether certain observed features, not explicitly reported for flat-plate boundary layers, are a general

characteristic of all wall-bounded flows or an effect of transverse curvature. Furthermore, the observed similarity between the cylindrical and flat plate boundary layers may be due to the moderate transverse curvature of the boundary layer used in this investigation (i.e. $\delta/a = 5$). Previous studies with much larger values of δ/a have indicated that the large-scale structures can move relatively freely throughout the boundary layer owing to less constraint by the wall. Bull & Dekkers (1993), for instance, reported observing crossflow fronts of low-speed fluid that sweep by the surface of the cylinder, stripping low-speed fluid from the wall in cylindrical boundary layers with $\delta/a > 20$. Some evidence for such energetic large-scale motions is apparent in the present measurements. Compared with a flat-plate boundary layer, turbulence intensities are larger near the wall (possibly due to the passage of large-scale outer structures very near the wall), streamwise velocity skewness is more negative throughout the boundary layer (possibly due to low-speed fluid stripped from the wall by the large-scale structure), and first-moment streamwise velocity spectra contain a greater fraction of the total energy near the spectral peak (which is presumably associated with the large-scale motion). However, it is not possible to say whether, for large transverse curvature ratios, the large-scale turbulence structure is merely 'enhanced' or fundamentally altered. Certainly, for moderate transverse curvature ratios such as that used in the present investigation, the fundamental character of the turbulence structure is not changed.

This research was funded by the Office of Naval Research under Contract No. N0014-89-J-1439, Mr James A. Fein, Program Manager with the support of Dr David Hurdis, Naval Undersea Warfare Center Detachment, New London, CT. Dr S. Snarski (currently employed with the Naval Undersea Warfare Center Detachment) was supported by an Amoco Foundation Doctoral Fellowship while at Northwestern University. The authors gratefully acknowledge the helpful comments provided by the reviewers.

REFERENCES

AFZAL, N. & SINGH, K. P. 1976 Measurements in an axisymmetric turbulent boundary layer along a circular cylinder. *Aero. Q.* **27**, 217–228.

BENDAT, J. S. & PIERSOL, A. G. 1986 *Random Data Analysis and Measurement Procedures.* John Wiley & Sons.

BLACKWELDER, R. F. & HARITONIDIS, J. H. 1983 Scaling of the bursting frequency in turbulent boundary layers. *J. Fluid Mech.* **132**, 87–103.

BLACKWELDER, R. F. & KAPLAN, R. E. 1976 On the wall structure of the turbulent boundary layer. *J. Fluid Mech.* **76**, 89–112.

BRADSHAW, P. 1967 Irrotational fluctuations near a turbulent boundary layer. *J. Fluid Mech.* **27**, 209–230.

BRADSHAW, P. 1971 *An Introduction to Turbulence and its Measurement*, p. 143. Pergamon.

BROWN, G. L. & THOMAS, A. S. W. 1977 Large structure in a turbulent boundary layer. *Phys. Fluids* **20**, S243–S252.

BULL, M. K. 1967 Wall-pressure fluctuations associated with subsonic turbulent boundary layer flow. *J. Fluid Mech.* **28**, 719–754.

BULL, M. K. & DEKKERS, W. A. 1993 Effects of transverse curvature on flow mechanisms in turbulent boundary layers. In *Near-Wall Turbulent Flows* (ed. R. M. C. So, C. G. Speziale & B. E. Launder), pp. 931–938, Elsevier.

BULL, M. K. & THOMAS, S. W. 1976 High frequency wall-pressure fluctuations in turbulent boundary layers. *Phys. Fluids* **19**, 597–599.

BULLOCK, K. J., COOPER, R. E. & ABERNATHY, F. H. 1978 Structural similarity in radial correlations and spectra of longitudinal velocity fluctuations in pipe flow. *J. Fluid Mech.* **88**, 585–608.

COLES, D. 1955 The law of the wall in turbulent shear flow. In *50 Jahre Grenzschichtforschung* (ed. H. Görtler & W. Tollmien), pp. 153–163. Vieweg & Sohn.

COLES, D. 1956 The law of the wake in the turbulent boundary layer. *J. Fluid Mech.* **1**, 191–226.

CORKE, T. C., NAGIB, H. M. & GUEZENNEC, Y. 1981 A new view on origin, role and manipulation of large scales in turbulent boundary layers. *IIT Fluids and Heat Transfer Rep.* R81-3. Illinois Institute of Technology, Chicago, IL.

DINKELACKER, A. 1990 Relations between wall pressure fluctuations and velocity fluctuations in turbulent pipe flow. In *Near-Wall Turbulence: Proc. 1988 Zoran Zaric Memorial Conference* (ed. S. J. Kline & N. H. Afgan), pp. 348–360. Hemisphere.

DINKELACKER, A. & LANGEHEINEKEN, T. 1983 Relations between wall pressure fluctuations and velocity fluctuations in turbulent flow. In *Structure of Complex Turbulent Shear Flows* (ed. R. Dumas & L. Fulachier), *IUTAM Symp., Marseille 1982*, pp. 1–9. Springer.

ECKELMANN, H. 1990 A review of knowledge on pressure fluctuations. In *Near-Wall Turbulence: Proc. 1988 Zoran Zaric Memorial Conference* (ed. S. J. Kline & N. H. Afgan), pp. 328–347. Hemisphere.

EMMERLING, R. 1973 Die momentane Struktur des Wanddruckes einer turbulenten Grenzschichtströmung. *Mitt. Max-Planck-Institut fur Strömungsforschung, u. Aerodyn. Vers., Göttingen*, no. 56.

FARABEE, T. M. 1986 *An experimental investigation of wall pressure fluctuations beneath non-equilibrium turbulent flows. DTNSRDC Tech. Rep.* 86/047. David Taylor Naval Ship Research and Development Center, Bethesda, MD.

FARABEE, T. M. & CASARELLA, M. J. 1991 Spectral features of wall pressure fluctuations beneath turbulent boundary layers. *Phys. Fluids* A **3**, 2410–2420.

FIEDLER, H. E. 1986 Coherent structures. In *Advances in Turbulence* (ed. G. Comte-Bellot & J. Mathieu), p. 320. Springer.

GEDNEY, C. & LEEHEY, P. 1989 Wall pressure fluctuations during transition on a plate. In *Symp. on Flow Induced Noise Due to Laminar-Turbulent Transition Process, ASME, NCA*, Vol. 5.

HARITONIDIS, J. H., GRESKO, L. S. & BREUER, K. S. 1990 Wall pressure peaks and waves. In *Near-Wall Turbulence: Proc. 1988 Zoran Zaric Memorial Conference* (ed. S. J. Kline & N. H. Afgan), pp. 397–417. Hemisphere.

HEAD, M. R. & BANDYOPADHYAY, P. 1981 New aspects of turbulent boundary-layer structure. *J. Fluid Mech.* **107**, 297–338.

HEAD, M. R. & RAM, V. V. 1971 Simplified presentation of Preston tube calibration. *Aero. Q.* **22**, 295–300.

HINZE, J. O. 1975 *Turbulence*, 2nd edn, pp. 673–677. McGraw-Hill.

JOHANSSON, A. V. & ALFREDSSON, H. P. 1982 On the structure of turbulent channel flow. *J. Fluid Mech.* **122**, 295–314.

JOHANSSON, A. V. & ALFREDSSON, H. P. 1983 Effects of imperfect spatial resolution on measurements of wall bounded turbulent shear flows. *J. Fluid Mech.* **137**, 409–421.

JOHANSSON, A. V., HER, J. & HARITONIDIS, J. H. 1987 On the generation of high-amplitude wall-pressure peaks in turbulent boundary layers and spots. *J. Fluid Mech.* **175**, 119–142.

KARANGELEN, C. C., WILCZYNSKI, V. & CASARELLA, M. J. 1991 Large amplitude wall pressure events beneath a turbulent boundary layer. In *Flow Noise Modeling, Measurement and Control* (ed. T. M. Farabee, W. L. Keith & R. M. Lueptow), *ASME, NCA*, Vol. 11/*FED*, Vol. 130, pp. 45–53.

KEITH, W. L., HURDIS, D. A. & ABRAHAM, B. M. 1992 A comparison of turbulent boundary layer wall-pressure spectra. *Trans. ASME* I: *J. Fluids Engng* **114**, 338–347.

KIM, J. 1983 On the structure of wall bounded turbulent flows. *Phys. Fluids* **26**, 2088–2097.

KIM, J. 1989 On the structure of pressure fluctuations in simulated turbulent channel flow. *J. Fluid Mech.* **205**, 421–451.

KLEBANOFF, P. S. 1957 Characteristics of turbulence in a boundary layer with zero pressure gradient. *NACA Rep.* 1247.

KLINE, S. J. & ROBINSON, S. K. 1990 Quasi-coherent structures in the turbulent boundary layer: Part

I. Status report on a community-wide summary of the data. Summary lecture in *Near-Wall Turbulence: Proc. 1988 Zoran Zaric Memorial Conference* (ed. S. J. Kline & N. H. Afgan), pp. 200–217. Hemisphere.

KOBASHI, Y., KOMODA, H. & ICHIJO, M. 1984 The wall pressure fluctuation and the turbulent structure of a boundary layer. In *Turbulence and Chaotic Phenomena in Fluids* (ed. T. Tatsumi), pp. 461–466, Elsevier.

KOBASHI, Y. & ICHIJO, M. 1986 Wall pressure and its relation to turbulence structure of a boundary layer. *Exps. Fluids* **4**, 49–55.

KOBASHI, Y. & ICHIJO, M. 1990 Relation between wall pressure and turbulence structure. In *Near-Wall Turbulence: Proc. 1988 Zoran Zaric Memorial Conference* (ed. S. J. Kline & N. H. Afgan), pp. 361–367. Hemisphere.

LAUFER, J. 1972 Recent developments in turbulent boundary layer research. *Instituto Nazionale di Alta Matematica, Symposia Matematica*, **9**, 299.

LU, S. S. & WILLMARTH, W. W. 1973 Measurements of the structure of the Reynolds stress in a turbulent boundary layer. *J. Fluid Mech.* **60**, 481–511.

LUEPTOW, R. M. 1986 The turbulent boundary layer on a cylinder in axial flow. ScD dissertation, Department of Mechanical Engineering, MIT, Cambridge, MA.

LUEPTOW, R. M. 1988 Turbulent boundary layer on a cylinder in axial flow. *NUSC Tech. Rep.* 8389. Naval Underwater Systems Center, New London, CT.

LUEPTOW, R. M. 1990 Turbulent boundary layer on a cylinder in axial flow. *AIAA J.* **28**, 1705–1706.

LUEPTOW, R. M. 1993 Wall pressure transducer spatial resolution. In *Flow Noise Modeling, Measurement and Control* (ed. T. M. Farabee, W. L. Keith & R. M. Lueptow), *ASME 1993 Winter Annual Meeting, New Orleans, NCA*, Vol. 15/*FED*, Vol. 168, pp. 49–55.

LUEPTOW, R. M. & HARITONIDIS, J. H. 1987 The structure of the turbulent boundary layer on a cylinder in axial flow. *Phys. Fluids* **30**, 2993–3005.

LUEPTOW, R. M. & JACKSON, C. P. 1991 Near-wall streaky structure in a turbulent boundary layer on a cylinder. *Phys. Fluids* A **3**, 2822–2824.

LUEPTOW, R. M., LEEHEY, P. & STELLINGER, T. 1985 The thick, turbulent boundary layer on a cylinder: Mean and fluctuating velocities. *Phys. Fluids* **28**, 3495–3505.

LUXTON, R. E., BULL, M. K. & RAJAGOPALAN, S. 1984 The thick turbulent boundary layer on a long fine cylinder in axial flow. *Aero. J.* **88**, 186–199.

MOIN, P. & KIM, J. 1985 The structure of the vorticity field in turbulent channel flow. Part 1. Analysis of instantaneous fields and statistical correlations. *J. Fluid Mech.* **155**, 441–464.

NEVES, J. C., MOIN, P. & MOSER, R. D. 1991 Numerical study of axial turbulent flow over a long cylinder. *8th Symp. on Turbulent Shear Flows, Munich, Germany (Sept. 9–11)*, pp. 1–6.

NEVES, J. C., MOIN, P. & MOSER, R. D. 1992 Numerical study of axial turbulent flow over long cylinders. *Stanford University Rep.* TF-54.

PANTON, R. L., GOLDMAN, A. L., LOWERY, R. L. & REISCHMAN, M. M. 1980 Low-frequency pressure fluctuations in axisymmetric turbulent boundary layers. *J. Fluid Mech.* **97**, 299–319.

PATEL, V. C. 1965 Calibration of a Preston tube and limitations on its use in pressure gradients. *J. Fluid Mech.* **23**, 185–208.

PERRY, A. E. & ABELL, C. J. 1975 Scaling laws for pipe-flow turbulence. *J. Fluid Mech.* **67**, 257–271.

PRESTON, J. H. 1954 The determination of turbulent skin friction by means of pitot tubes. *J. R. Aero. Soc.* **58**, 109.

RICHMOND, R. L. 1957 Experimental investigation of thick, axially symmetric layers on cylinders at subsonic and hypersonic speeds. *Hypersonic Research Proj. Memo* 39. California Institute of Technology, Pasadena, CA.

ROBINSON, R. L. 1990 A review of vortex structures and associated coherent motions in turbulent boundary layers. In *Structure of Turbulence and Drag Reduction IUTAM Symp. Zurich, Switzerland, 1989* (ed. A. Gyr), pp. 23–50. Springer.

ROBINSON, S. K., KLINE, S. J. & SPALART, P. R. 1990 Quasi-coherent structures in the turbulent boundary layer: Part II. Verification and new information from a numerically simulated flat-plate layer. Summary lecture in *Near-Wall Turbulence: Proc. 1988 Zoran Zaric Memorial Conference* (ed. S. J. Kline & N. H. Afgan), pp. 218–247. Hemisphere.

RUSSELL, S. J. & FARABEE, T. M. 1991 The wall pressure field due to a wing-body flow. In *Flow Noise*

Modeling, Measurement and Control (ed. T. M. Farabee, W. L. Keith & R. M. Lueptow), *ASME, NCA*, Vol. 11/*FED*, Vol. 130, pp. 85–94.

SAMUEL, A. E. & JOUBERT, P. N. 1974 A boundary layer developing in an increasingly adverse pressure gradient. *J. Fluid Mech.* **66**, 481–505.

SCHEWE, G. 1983 On the structure and resolution of wall-pressure fluctuations associated with turbulent boundary-layer flow. *J. Fluid Mech.* **134**, 311–328.

SHAH, D. A. & ANTONIA, R. A. 1989 Scaling of the 'bursting' period in turbulent boundary layer and duct flows. *Phys. Fluids* A **1**, 318–325.

SNARSKI, S. R. 1992 Relation between the fluctuating wall pressure and the turbulent structure of a boundary layer on a cylinder in axial flow. PhD dissertation, Department of Mechanical Engineering, Northwestern University, Evanston, IL.

SNARSKI, S. R. 1993 Relation between the fluctuating wall pressure and the turbulent structure of a boundary layer on a cylinder in axial flow. *NUWC TR* 10223, Naval Undersea Warfare Center Detachment, New London, CT.

SPALART, P. R. 1988 Direct simulation of a turbulent boundary layer up to $R_\theta = 1410$. *J. Fluid Mech.* **187**, 61–98.

STRICKLAND, J. H. & SIMPSON, R. L. 1975 Bursting frequencies obtained from wall shear stress fluctuations in a turbulent boundary layer. *Phys. Fluids* **18**, No. 3, 306–308.

THOMAS, A. S. W. & BULL, M. K. 1983 On the role of wall-pressure fluctuations in deterministic motions in the turbulent boundary layer. *J. Fluid Mech.* **128**, 283–322.

WHITE, F. M. 1972 An analysis of axisymmetric turbulent flow past a long cylinder. *Trans. ASME* D: *J. Basic. Engng* **94**, 200–206.

WHITE, F. M. 1974 *Viscous Fluid Flow*, pp. 554–558. McGraw Hill.

WIETRZAK, A. & LUEPTOW, R. M. 1994 Wall shear stress and velocity in a turbulent, axisymmetric boundary layer. *J. Fluid Mech.* **259**, 191–218.

WILCZYNSKI, V. & CASARELLA, M. J. 1992 Correlations between organized turbulent structures and wall pressure fluctuations. In *Symposium on Flow-Induced Vibration and Noise*, *ASME, NCA*, Vol. 13, pp. 165–180.

WILLMARTH, W. W. 1975*a* Structure of turbulence in boundary layers. *Adv. Appl. Mech.* **15**, 159–254.

WILLMARTH, W. W. 1975*b* Pressure fluctuations beneath turbulent boundary layers. *Ann. Rev. Fluid Mech.* **7**, 13–38.

WILLMARTH, W. W. & ROOS, F. W. 1965 Resolution and structure of the wall pressure field beneath a turbulent boundary layer. *J. Fluid Mech.* **22**, 81–94.

WILLMARTH, W. W. & SHARMA, L. K. 1984 Study of turbulent structure with hot wires smaller than the viscous length. *J. Fluid Mech.* **142**, 121–149.

WILLMARTH, W. W. & TU, B. J. 1967 Structure of turbulence in the boundary layer near the wall. *Phys. Fluids Suppl.* **10**, S134–S137.

WILLMARTH, W. W., WINKEL, R. E., SHARMA, L. K. & BOGAR, T. J. 1976 Axially symmetric turbulent boundary layers on cylinders: mean velocity profiles and wall pressure fluctuations. *J. Fluid Mech.* **76**, 35–64.

WILLMARTH, W. W. & WOOLDRIDGE, C. E. 1962 Measurements of the fluctuating pressure at the wall beneath a thick turbulent boundary layer. *J. Fluid Mech.* **14**, 187–210.

WILLMARTH, W. W. & WOOLDRIDGE, C. E. 1963 Measurements of the correlation between the fluctuating velocities and the fluctuating wall pressure in a thick turbulent boundary layer. *AGARD Rep.* 456.

WILLMARTH, W. W. & YANG, C. S. 1970 Wall-pressure fluctuations beneath turbulent boundary layers on a flat plate and a cylinder. *J. Fluid Mech.* **41**, 47–80.

YUAN, Y. M. & MOKHTARZADEH-DEHGHAN, M. R. 1994 A comparison study of conditional-sampling methods used to detect coherent structures in turbulent boundary layers. *Phys. Fluids* **6**, 2038–2057.